NOVA SCHOOL OF
SCIENCE & TECHNOLOGY

DEPARTMENTO DE
CIÊNCIA DOS MATERIAIS

**MARIA TERESA OLIVEIRA PULQUÉRIO DE SILVEIRA**

Licenciada em Engenharia de Materiais

# 3D PRINTING OF YBCO-BASED SUPERCONDUCTORS

MESTRADO EM ENGENHARIA DE MATERIAIS

Universidade NOVA de Lisboa
Dezembro, 2021

NOVA SCHOOL OF SCIENCE & TECHNOLOGY

DEPARTAMENTO DE CIÊNCIAS DOS MATERIAIS

# 3D PRINTING OF YBCO-BASED SUPERCONDUCTORS

**MARIA TERESA OLIVEIRA PULQUÉRIO DE SILVEIRA**
Licenciada em Engenharia de Materiais

**Orientador:** Isabel Maria das Mercês Ferreira
*Associate Professor with Aggregation, NOVA University Lisbon*

**Jurí:**

**Presidente:** Alexandre José da Costa Velhinho
*Auxiliar Professor, NOVA University Lisbon*

**Vogais:** João Pedro Botelho Veiga
*Associate Professor, NOVA University Lisbon*

MESTRADO EM ENGENHARIA DE MATERIAIS
Universidade NOVA de Lisboa
Dezembro, 2021

**3D printing of YBCO-based superconductors**

*To my family.*

# Acknowledgements

First, I'd like to thank Professor Isabel Ferreira for all the knowledge that she has passed to me, for the opportunity of doing my thesis with her team and for all her patience.
Second I would like to thank David for all the discussions, for his patience and for always trying to make me do better and see a little bit beyond what I would typically do. You made me a better person in and out of the work environment.
I would also like to thank Ana Marques, Andreia, Professor João Canejo, Professor Rita Branquinho, Professor Carmo Lança and Professor Maria Rolim not only for helping me with knowledge and equipments but also for always being available and kind. Regarding the people in the lab, I would like to thank Catarina, Miguel, Margarida, Iris, Mariana, Inês, Cabral and both Joãos for all the help making my day a little bit better.
I would like to thank my friends that always have been here for me, first, the ones that have been here all along and that have been great in keeping me grounded I would like to thank Nena, Gugas, Salomé, Dádá, Piolho and Miranda. For my university friends I would like to thank first, my firsts ones, Clau, Galamba, Kevin and Silvano, who have been with me (almost) since day one and have been a great strenght for me. Lastly, I would like to thank Guixa, Moki, Tavares, Pedro, Ana and Paty whom have made the last 4 years the best ones and with whom I can't live without anymore.
Finally, I would like to show my gratitude towards my family in portuguese. Agradeço muito aos meus avós (Noémia, António e Emilia) e aos meus tios, tanto os de sangue como os que não o são por terem estado sempre presentes na minha vida e por me terem sempre tentado ajudar em tudo o que pudessem. Por fim gostaria de agradecer aos meus pais, irmão, namorado e a duas pessoas muito especiais que se tornaram parte da familia (Duarte e Sophie) que sempre me encorajaram em tudo e me mantiveram otimista e focada em momentos que achei que o mesmo não seria possível. Sem todos vocês não teria sido possível ter chegado onde cheguei!
Muito obrigada! Thank you all!

# Abstract

The importance superconductors have in energy applications and their high fabrication cost led to the necessity of developing a recycling method to reduce their environment footprint. Yttrium Barium Copper Oxide (YBCO), a well known superconductor, was chosen to test the method. Doping with Ca, Fe and graphene was also attempted to improve its superconducting properties. For the synthesis of YBCO, conditions such as the influence of sintering time and temperature and the influence of milling time were tested. Optimal conditions for the synthesis of superconducting YBCO were not achieved, probably due to a short sintering time. The recycling process was divided into two steps: sintering at 900 °C for 16 hours and then milling for 180 minutes. 3D printing was tested for both synthesized and recycled powders. The elements used to dope the YBCO at the tested concentrations did not show superconducting properties. The properties of synthesized, recycled and doped YBCO were evaluated using scanning electron microscope imaging, Raman spectroscopy, X-ray diffraction analysis, electric measurements and levitation tests.
Longer sintering times and different doping concentrations should be tested in future works to achieve better superconducting properties.

**Keywords:** YBCO, 3D Printing, Recycling, Doping

# Resumo

A importância que os supercondutores têm em aplicações relacionadas com energia e o seu elevado custo de fabrico, levaram à necessidade do desenvolvimento de um método de reciclagem de modo a diminuir a sua pegada ambiental. O óxido de ítrio, bário e cobre (YBCO) é um supercondutor bastante estudado, sendo por isso o escolhido para testar o método. A dopagem com Ca, Fe e grafeno foi também testada de modo a melhorar as propriedades supercondutoras. Para a síntese de YBCO estudou-se a influência do tempo e temperatura de sinterização e também o tempo de moagem. As condições ótimas para a síntese de YBCO supercondutor não foram conseguidas, provavelmente devido aos baixos tempos de sinterização escolhidos. O processo de reciclagem foi dividido em dois passos: sinterização a 900 °C por 16 horas e moagem por 180 minutos. A impressão 3D foi realizada tanto para pós sintetizados como reciclados. Os elementos utilizados na dopagem de YBCO, nas concentrações escolhidas, não demonstraram ser eficazes na obtenção de propriedades supercondutoras. As propriedades dos pós de YBCO sintetizados, reciclados e dopados foram avaliadas utilizando microscopia eletrónica de varrimento, espectroscopia de Raman, difração de raios X, medidas elétricas e testes de levitação.
Como principal conclusão, o tempo de sinterização dos pós e outras concentrações de dopagem devem ser testadas em futuros trabalhos de modo a verificar se de facto estes elementos possibilitam a melhoria das propriedades supercondutoras.

**Palavras-chave:** YBCO, Impressão 3D, Reciclagem, Dopagem

# Contents

# List of Figures

# List of Tables

# Acronyms

**DMF** Dimethylformamide.

**FC** Field cooling.

**GO** Graphene oxide.

**$H_C$** Critical external magnetic field intensity.

**$J_C$** Critical current density.

**NFA** Heating treatment for 29 hours.

**NFN** Heating treatment for 16 hours.

**NFP** Heating treatment for 6 hours.

**PS** Polystyrene.

**PVA** Poly(vinyl alcohol).

**PVDF** Poly(vinylidene fluoride).

**rGO** Reduced graphene oxide.

**SDS** Sodium dodecyl sulfate.

**SEM** Scanning electron microscope.

**SQUID** Superconducting quantum interference device.

**$T_C$** Critical temperature.

**XRD** X-ray diffraction.

**Y123** YBCO 123.

**Y211** YBCO 211.

**YBCO** Yttrium barium copper oxide.

**ZFC** Zero field cooling.

Chapter 1

# Introduction

## 1.1 Superconductors

Superconductivity was firstly discovered in 1911 by Heike Kamerlinght Onnes while studying the electrical properties of frozen mercury, discovering that its electrical resistance decreased from $10^{-1}$ to $10^{-5}$ Ω near 4.2K [1]. It has been defined a critical temperature ($T_C$) to which this phenomenon is manifested and is reversible, meaning that above this temperature the resistance recovers its previous values [1]. An extensive investigation on the field led to the appearance of a variety of materials such as alloys, pure metals, binary and ternary compounds and organic materials. This led to the discovery of superconductor materials with higher $T_C$ [1].
In 1986, Karl Alex Müller and George Bednorz discovered the first superconductor material with $T_C$ above 35K, $La_2CuO_4$ [2]. In 1987, by substituting $La^{3+}$ by $Y^{3+}$ it was possible to discover the first material to have $T_C$ above the boiling temperature of nitrogen [2]. This discovery raised hope and increased the research on the area, focusing on materials with even higher $T_C$ values [1],[3]. In Figure 1.1, it is possible to observe the advances made regarding the research of superconductors.

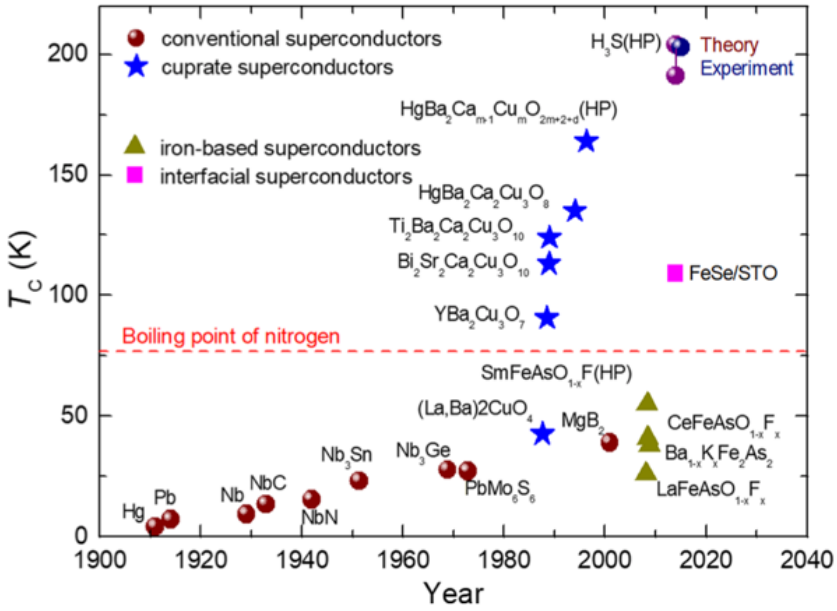


Figure 1.1: Evolution up to 2020 of main superconductor materials [4].

### 1.1.1 Superconductive State

Superconductors are frequently described as materials with zero electrical current resistance when under certain conditions, such as critical temperature ($T_C$), critical current density ($J_C$) and critical external magnetic field intensity ($H_C$) [5]. $J_C$ is the maximum current that the superconductor can carry, and $H_C$ is the maximum magnetic field that the superconductor can endure before returning to a non-superconductive state. Figure 1.2 shows a representation of how the superconductive state is influenced by temperature, current density and magnetic field [6]. In 1933 it was discovered that if a material was placed in a magnetic field, while at a temperature

below its $T_C$, that the field would be expelled from its interior [1]. However, if the magnetic field applied was higher than $H_C$ or if the temperature was higher than $T_C$, the material would revert to a normal conductor [1]. The phenomenon of magnetic field expulsion is called the Meissner effect and correlates the perfect diamagnetism that is exhibited by the material when the magnetic field applied and the temperature is below a certain critical value [1].

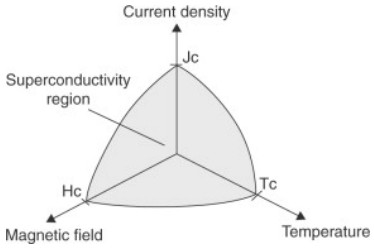


Figure 1.2: Limits of the superconductive state [6].

The discovery of superconductor materials with higher $T_C$, also induced the discovery that, those materials might behave differently with the magnetic field, creating the classes of type I and type II superconductors [7]. In type I the normal state is attained abruptly for a given critical magnetic field $H_C$. In type II, the magnetization drops before reaching $H_C$ [1]. There is some penetration of the flux in the specimen at a certain $H_{C1}$, creating vortexes, for values below $H_C$, maintaining its superconductive properties up to a field of $H_{C2}$, with a value above $H_C$ [1]. Above $H_{C2}$, the material will begin to behave like a normal conductor, as can be seen in Figure 1.3 A and Figure 1.3 B [1]. It is important to note that, as London discovered, the magnetic flux lines, in both types of superconductors, will not be completely expelled from the superconductor but instead will remain confined in a thin surface layer called penetration depth that can be observed in Figure 1.3 C [1].

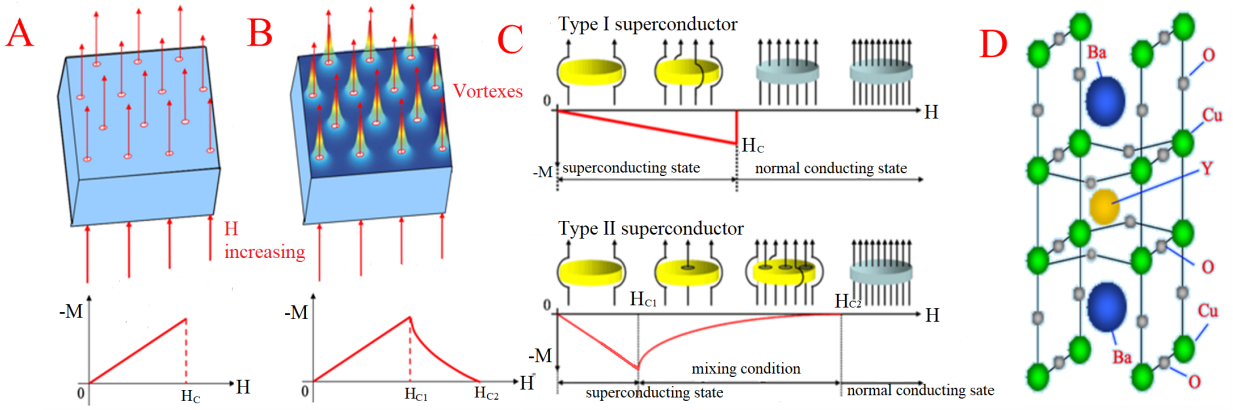


Figure 1.3: A - Type I and B - Type II superconductors, C - Schematics of magnetic line flux in type I and type II superconductors, D - YBCO perovskite structure [8],[9].

The current transport on superconductors type I is made by the Cooper pairs. As the temperature decreases, the electrons with energy close to the Fermi level will interact with the ion-lattice, due to the reduced scattering at low temperatures, causing the current to continue flowing and have no incoherent scattering [1]. When the pairs are formed, the two electrons have zero net momentum and opposite spins, causing the current flow not to change and then having incoherent scattering [1]. The only scattering event that will reduce the current occurs when the pair has energy greater than its binding energy [1]. For current densities below $J_C$, the energy will not be surpassed, and there will not be any loss of current during the transport [1]. For superconductors

type II, there is also a carrier pairing, like plasmons, exitons or magnons, and an energy gap, however, it is still not known which excitations are responsible for the inter-electron attraction [1].
The temperature is the most important parameter that regulates the superconductive state, it affects the value of $H_C$, determine if the flux will penetrate the material and the formation of Cooper pairs [1].

### 1.1.2 Yttrium Barium Copper Oxide

In 1987, Paul Ching-Wu, Maw-Kuen Wu and their fellow co-workers discovered, by modificating original oxides, a new kind of type II superconductors: the Yttrium Barium Copper Oxide (YBCO), with a $T_C$=91K [1],[3],[10]. Its structure is similar to the one of a perovskite, with sheets of copper and oxygen atoms alternated with sheets of yttrium and oxygen atoms [1]. In Figure 1.3 D it can be seen the orthorhombic form of YBCO [1]. The unit cell contains one layer of the metallic cation copper surrounded by four oxygen ions (Cu 1), a layer of barium oxide, another layer of copper surrounded by five oxygen ions (Cu 2) and a layer of yttrium, short of four oxygen atoms. The presence of the double $CuO_2$ layer is what it is believed to be the key to the occurrence of the superconductive sate in these kind of oxides [1].
The general formula of YBCO is $YBa_2Cu_3O_7-x$ in which x takes values between 0 and 1. If the value of x is equal to 0, the structure will be orthorhombic, as can be seen in Figure 1.3 D, if the value is higher than 0.6, the structure will change to tetragonal. The unit cell parameters and the $T_C$ will also be influenced by x and the value of $T_C$=91K is only possible for values below 0.2 [1]. With its ceramic nature, YBCO will have brittle behavior which will make the production of complex geometries difficult [10].
The previous form of YBCO is known as YBCO 123 ($YBa_2Cu_3O_7$) but it is also possible to obtain other forms of YBCO, such as YBCO 211 ($Y_2BaCuO_5$) that is obtained when the synthetization temperature goes above 1030 °C. This material does not possess superconducting properties but is believed to act as a pinning center for vortices and thus increases the $J_C$ [11],[12]

### 1.1.3 Applications

The production of superconductors will depend on the desired shape (wires, thins films or bulk materials), and the desired final application [7],[13]. Some of the applications for superconductivity can be referred in Table 1.1 [1]. For other applications, namely the ones specifically for high temperature superconductors, may refer to the work of Mendes et al.[7] as well as Saxena et al.[1] and Wei et al.[14].

Table 1.1: Different applications for superconductive materials.

| Basis | Application |
|---|---|
| R=0 and high $J_C$ | 1.Magnets |
| | 2.Passive microwave devices |
| | 3.Interconnects in microelectronics |
| | 4.Electrical energy transport by cables |
| Josephson tunneling | 1.Microwave detectors and mixers |
| | 2.Physical measurements (like SQUID) |
| | 3.Computers for fast logic and memory circuits |
| | 4.Plasma and space |
| | 5.Medicine (magnetoencephalography) |
| High $J_C$ and high $H_C$ | 1.Electrical power industry |
| | 2.Plasma confinement for high energy physics |
| | 3.Transport (levitation trains or MHB-propelled ships) |
| | 4.Medicine (nuclear magnetic resonance tomography |

The techniques that may be used to produce superconductors are solid state reactions, solution techniques or plasma synthesis [10]. Some examples are: melt texture processing [15], sputtering deposition [16], electrophoretic deposition [17], spraying techniques [18], laser sintering [19], plastic extrusion [20], top-seed melting texturing method [21], melt texture growth method [22], powder melting process [23], chemical vapor deposition [24], thermal evaporation [25], chemical solution deposition [26] and extrusion based 3D printing [10].

## 1.2 Sustainability Issue

Considering the current world situation regarding pollution it is important to be conscious and to try approaches that will have the most environmentally friendly outcome possible.

### 1.2.1 Waste generated by 3D printing and superconductor industry

Additive manufacturing or 3D printing is a process in which an object will be built by printing layers on top of layers until the final design is achieved [27]. This process allows the production of complex geometries and will not require further machining or reprocessing [10]. In recent years, the usage of 3D printing has become more popular in diverse industrial sectors such as aerospace, military, automotive, medical and construction [28]. Since 3D printing has lower cost, higher simplicity and almost limitless freedom of design when compared with other manufacturing techniques, it has been used not only for the final products but also for prototyping, leading to the generation of an immense amount of material waste [14],[28],[29].
The superconductor industry is also a big producer of waste, with failure rates as high as 30% [30]. In this sector, since the manufacture price is high, the usage of 3D printing technology would be beneficial considering that it would allow lower production costs when compared to other techniques, allowing for a reduction and perhaps recover of the waste generated [31]. With 3D printing technology, there could be a possibility to use previously discarded materials, such as YBCO, to be used as new ink, making it possible to recycle the material that would be going to waste otherwise.

### 1.2.2 Material mining

Mining activities, starting at prospecting, and ending in abandonment, impact social and environmental systems, contributing to erosion, sinkholes, deforestation, loss of biodiversity, water

pollution, acid mine drainage and contamination of the soil, ground and surface water [32],[33]. In addition to the environmental issues that mining causes, all of them, direct on indirectly, lead to health issues in local populations and on the miners, as well as serving as a fuel for civil wars [33],[34].
All the materials that will be used in this project to form YBCO ($Y_2O_3$, $BaCO_3$, BaO and CuO) were once part of a mineral that was mined, contributing to the necessity to continue to extract these non-renewable resources.

## 1.3 State of Art

Mendes et al.[10] used YBCO powders and printed them, comparing them afterwards with pieces made from a mix of $Y_2O_3$, $BaCO_3$ and CuO. The work done showed that it was possible to obtain the orthorhombic phase of a 3D printed YBCO structure, using a paste extruder, with the desired geometry and superconducting properties. Wei et al.[29] also proved that it was possible to print YBCO paste with extrusion freeforming, coupled with a post sintering process for bulk application and Wei et al.[14] demonstrated that, when comparing milled and unmilled dust, that, the milled powder has higher critical current density and mechanical strength due to the densification process. In the mentioned study it was also possible to see that, due to the material's high chemical homogeneity and specific surface area, that is was possible to obtain YBCO 123 at lower temperatures.
Iida et al.[31] used recycled milled precursor powder from failed GdBCO/Ag to form pellets and, with chemical analysis, proved that it was not significantly different from the commercial mixtures available, using afterwards the hot seeding technique. This proved that it is possible to recycle GdBCO/Ag, however it is important to mention that there was a small degradation on the superconductor properties. Xu et al.[30] used cold seeding melt texture growth as it would allow for lower temperatures and it would prevent decomposition that could occur at higher temperatures. With this work it was proven the possibility of recycling failed bulks of YBCO.
Since it has been proven that it is both possible to print YBCO using a paste extruder and to recycle YBCO and other superconductors, this dissertation will focus on the possibility of recycle previously printed designs of YBCO without the degradation of superconductive properties. It will also be desired to increase the magnetization temperature which will be tried with the addition of reduced graphene oxide (rGO) and $Fe_2O_3$ nanoparticles and $CaCl_2$ since there are proof, regarding rGO, of a rise of the critical temperature [35].
Material doping is an important step to obtain better properties for the final material. Graphene oxide (GO) is a promising material with numerous applications due to its thermal, electrical and mechanical characteristics, being a good candidate as an additive material [36]. Gaffoor et al. [35] proved that the addiction of GO and reduced GO (rGO) leads to higher mechanical hardness due to solute solution strengthening and that, GO doped YBCO has higher $T_C$ values when compared to pure YBCO and to rGO doped YBCO.
Regarding weak bonds, that can lead to a decreasing critical transport current on the bulk YBCO and increase resistance in the normal state, Gaffoor et al. [35] states that the effect is most improved with concentrations of 0.7 wt% for both GO and rGO doped YBCO. This effect could be due to better pinning in the grain boundaries, since the particles seem to remain between the grains that act as weak bonds [35],[37]. There are several methods to increase $J_C$, one of which is to include nanoparticles as artificial defects [38]. Zhang et al.[38] and Abd-Ghani et al.[39] proved that, for certain concentrations, it is possible for the $T_C$ to decrease and for the $J_C$ to increase due to the presence of flux pinning centers. It is known that superconducting properties such as $T_C$ and $J_C$ are a function of the oxygen content, which controls the carrier concentration on the copper oxide planes [40]. One of the possible cation substitutes that will cause such impact is Ca substituting Y since the different valence states will introduce additional carriers [40]. Yao et al.[41] stated that $J_C$ decreases less in Ca doped YBCO when compared

with non-doped YBCO because the presence of Ca increases the carrier density. However, the $T_C$ decreases due to the overdoped regime and the increased disorder [42].

Chapter 2

# Methods and Materials

## 2.1 Materials

Two different powders' compositions were studied: A - Barium Carbonate ($BaCO_3$) (Honeywell Fluka, ≥99), Copper(II) Oxide nanopowder (CuO)(Sigma Aldrich) and Yttrium(III) Oxide ($Y_2O_3$) (Alfa Aesar, ≥99.99), and B - Barium Oxide (BaO) (Haihang industry), Copper(II) Oxide (CuO) (Haihang industry) and Yttrium(III) Oxide ($Y_2O_3$) (Haihang industry).
The materials used for the doped powders and for the pastes are referred in the Table A.1 and Table A.2 in the Appendix chapter's section Materials.

## 2.2 Methods

### 2.2.1 Powder Synthesis

The precursor powders with the formulations: barium carbonate, copper(II) oxide and yttrium(III) oxide (A) or barium oxide, copper(II) oxide and yttrium(III) oxide (B) were weighed and mixed with a molar proportion of: 1 mol of Y to 2 moles of Ba to 3 moles of Cu. The samples synthesized can be seen in the Table A.4 and Table A.5 of the Powders section of the Appendix chapter.
The mix was made with a coffee grinder or with a mortar until an homogeneous mixture was obtained. It was observed that the usage of a mortar allowed for more homogeneous samples with less YBCO 211 green phase present. Additionally, mixtures made with the coffee grinder did not retain their apparent homogeneity and white spots (possibly Y or Ba) started to appear over time.
The powder was later placed on a oven in order for the YBCO to be formed, using 900 °C for BaO [39] and 950 °C for $BaCO_3$ [7]. The complete description of the heating curves and temperatures, as well as the heating treatments' acronyms used, are stated in Table A.3 in the Methods section of the Appendix chapter.
The material was milled using Reutsch PM 100 for 10, 30, 60 and 180 minutes at 500rpm and the milled powder was used to print or for pellets' characterization. The pellets went into the oven for annealing for 16 hours (heating treatment NFN) at 900 °C.

### 2.2.2 Recycling

For the recycling cycles, the powders were annealed at 900 °C using NFN and then were milled for 180 minutes. The complete list of the recycled powders can be seen in Table A.6 of the Recycled Powders section of the Appendix chapter.

### 2.2.3 Doping

The samples synthesis was made similar to the non-doped samples but a small amount of dopant was added as shown in Table 2.1.

Table 2.1: Doping percentages used for the dopants tested.

| Doping Agent | Doping percentages/ wt% | Reference |
|---|---|---|
| $CaCl_2$ | 0.05, 0.1, 0.2 and 0.3 | [37] |
| $Fe_2O_3$ | 0.01, 0.02, 0.03, 0.04 and 0.05 | [39] |
| Reduced Graphene Oxide | 0.1, 0.3, 0.7 and 1 | [43] |

The powders for the synthesis of the YBCO and the doping element were mixed with a IKA ULTRA TURRAZ Tube drive control with 24 stainless steel balls for 30 minutes at 6000 rpm and then had an heating treatment for 16 hours (NFN) at 900 °C. A complete list of the doped powders can be seen in Table A.7 to Table A.9 in the Doped Powders section of the Appendix chapter.

### 2.2.4 Characterization

The samples were characterized to attain important information regarding its structure, constitution, and its electrical and superconducting properties.
It was used Spectrophotometer Jasco V-770 to obtain the reflectance spectrum. The pellets or powders were analyzed, and the reflectance results were normalized using Equation A.1 presented in Spectroscopy subsection of the Methods section of the Appendix Chapter. The results obtained from that will allow for a verification of the presence of the YBCO 211 green phase that can be seen as a peak near 500 nm. Witec Alpha 300 confocal RAS, with a 532 nm Argon Laser at 2.5 mW of power, was used to attain which phases and elements were present in the samples. YBCO pellets/powders were analyzed. Hitachi S2400, with Bruker light elements energy dispersive X-ray spectroscopy, was used to obtain photos of the different powders, via scanning electron microscopy (SEM). From the SEM images obtained, 80 random particles were selected and were analyzed via ImageJ to obtain their sizes. X'Pert PRO MPD, with a Cu K-α source (at the wavelength of 1.540598 Å) was used to obtain the material's structure. For that, YBCO powder was tested. To attain the material's conductivity, current and voltage were measured with the setup that can be seen in Figure A.1 A in the Electric Measurements subsection of the Methods section of the Appendix chapter. A complete explanation of the calculations of the conductivity is also described in the section mentioned before. Superconducting Properties $T_C$ and $J_C$ were obtained by a superconducting quantum interference device (SQUID), model S700X by Cryogenic LTd. YBCO pieces were used to obtain the graphs: magnetization versus temperature, magnetization versus magnetic field strength and $J_C$ versus magnetic field. In the magnetization versus temperature graph, it was used a 100G magnetic field. For the magnetization versus magnetic field strength it was tested different temperatures (77, 50, 10 and 4 K) and a magnetic field strength range from -6 to 6 T. For the $J_C$ versus magnetic field it was used different temperatures (77, 50, 10 and 4 K) and a magnetic field range of 0 to 6 T. Levitation tests were performed as a quick and easy way to check the material's superconducting properties. Those tests were done with liquid nitrogen and magnets (cylindrical neodymium with 2 cm diameter and cubic neodymium with 0.5 cm side). The schematics of the setup used is shown in Figure A.2 in the Magnetic Levitation subsection of the Methods section of the Appendix chapter.

Chapter 3

# Results

This chapter summarizes the results obtained for the different experiments performed, related to the influence of the choice of precursors, sintering temperature and time, milling time, the reproducibility and recyclability of samples made with sintered YBCO powders and the possibility of achieving better superconductor properties with doping.

## 3.1 Synthesis of YBCO

YBCO powders were produced by solid state reactions of precursors containing Y, Ba and Cu elements, with the mixtures and proportions referred in Methods and Materials chapter.
The sintering temperature was selected after literature review and the DSC/TG analysis. Some synthesis trials with different temperature values were also done. Then, the influence of milling time on the properties of YBCO was tested.

### 3.1.1 Influence of Temperature and Time

Different heat treatments were tried to achieve the optimized sintering time and temperature for the formation of YBCO 123. First, to find the optimum sintering temperature range DSC was performed in two different powder mixtures, A with $BaCO_3$, CuO and $Y_2O_3$, and B with BaO, CuO and $Y_2O_3$ . The results are shown respectively in Figure 3.1 A and B.

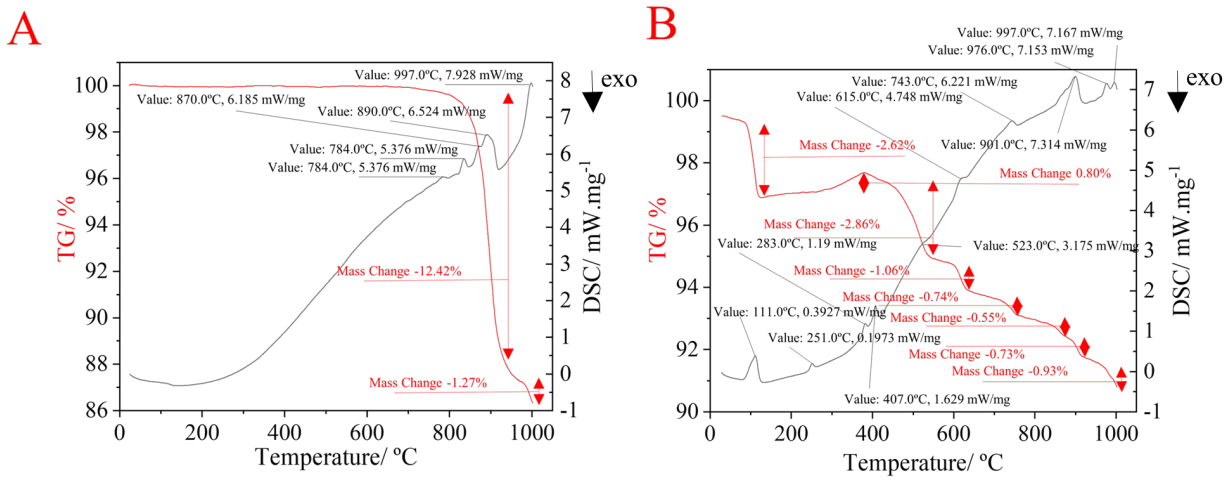


Figure 3.1: DSC/TG of YBCO made with A - mixture A (with $BaCO_3$) and B - mixture B (with BaO).

The sample of mixture A shows at around 900 °C, a sudden drop of mass corresponding to the carbonate transformation into $CO_2$ gas. Using the molar masses of $BaCO_3$, $Y_2O_3$, CuO, and YBCO it is possible to attain the the real value of percentage of mass that is lost and compare it to the real value. The value obtained was 22.46%, when compared with the experimental value (12.42%) it is possible to see that there was some part of the material (10.44%) that did not react, which could be due to the heating rate used being to fast (10K/min). The experimental data seems to indicate, according to what was expected, that the sintering temperature should be around 900 to 950 °C. The sample with B mixture shows a possible dehydration around 100

°C (2.62%) and a descarboxylation near 900 °C. By the same calculations that were done before, but with BaO instead of $BaCO_3$,it was obtained an expected drop of 13.61% in mass, which is almost double the experimental result (6.07%), once more, probably due to the heating rate used. It was not possible to obtain information regarding what those peaks correspond to in the literature review, but some may be due to the liberation of oxygen. Considering the DSC results and literature, the sintering temperature of the mixture A and B should be 950 °C and 900 °C respectively [7],[39]. Additionally, it was tried sintering at 1100 °C to prove the transition from YBCO 123 to YBCO 211 [44]. For this synthesis (O24), it was shown that the sample appeared to have high quantity of YBCO 211 green phase as can be seen by the peak at 500 nm in the normalized reflectance graph in Figure A.9 in Spectroscopy section in the Appendix chapter.
Samples of YBCO with mixtures A and B and a sample of YBCO 211 were analyzed via XRD. Figure 3.2 A shows the XRD diffractogram of a sample made with A mixture at 950 °C and B shows the diffractogram of a sample made with B mixture at 900 °C. The analysis was based on the work of Wei et al.[29]. Regarding the Figure's caption, Y123 O represents YBCO 123 with orthorhombic phase, Y123 T YBCO 123 with tetragonal phase and Y211 represents YBCO 211.

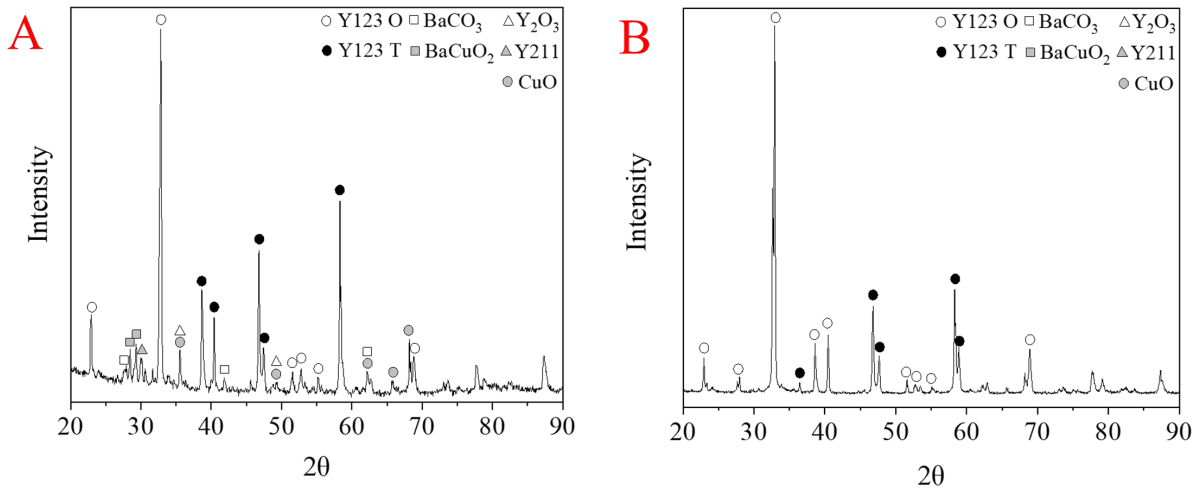


Figure 3.2: XRD pattern of YBCO sample made with A - A mixture ($BaCO_3$, $Y_2O_3$, CuO), B - B mixture (BaO, $Y_2O_3$, CuO).

The pattern of Figure 3.2 A corresponds majorly to YBCO 123 orthorhombic phase as its peaks intensity are predominant, however the presence of $Y_2O_3$, CuO and $BaCO_3$ precursors is also seen by the small peaks identified in the figure. Those peaks could be due to an ineffective mixture of the precursors' powders or an incomplete reaction. It is also possible to see the $BaCuO_2$ phase peaks. Regarding the observed phases, the tetragonal structure is shown by the peaks at 39°, 40°, 46 °, 47° and 58° and orthorhombic phase on the peak at 33°. Therefore, both tetragonal and orthorhombic phases are present in the sintered powder. The presence of the tetragonal phase might be due to the low oxygen content in the material's structure. In Figure 3.2 B the only phase present is YBCO 123, meaning the sintering time and temperature, and precursors' mixture were adequate. However, most of the peaks belong to the tetragonal structure, namely the ones at 33°, 47°, 48°, 58° and 59°. The peaks at 36°, 39° and 40° are due to orthorhombic structure suggesting that, yet again, there is a mixture of phases in the obtained powder.
Figure 3.3 A shows the XRD pattern of a sample made with A mixture at 950 °C, which formed YBCO 211 and YBCO 123. The visual aspect of the sample rich with 211 and the sample that did not possess it is given in Figure 3.3 B, one in black (YBCO 123) and the other containing green color regions (YBCO 211 + YBCO 123). This is also observed in XRD diffractogram as observed in Figure 3.3 A where the main peak corresponds to YBCO 123, but the precursors $Y_2O_3$, CuO and $BaCO_3$ are also present. The non-homogeneity of the precursor's powder mixture

can be due to an incomplete reaction between them. Licci et al.[44] also reported the presence of YBCO 211 by an oven's temperature overshoot leading to hotter sintering temperatures. It is difficult to discern the YBCO structure due to the presence of many peaks or precursors, however, some peaks characteristic of the orthorhombic structure such as the one at 33°, and some characteristics of the tetragonal structure such as the ones at 47°, 58° and 59° are observed. Therefore, the analyzed powder shows the presence of both phases.

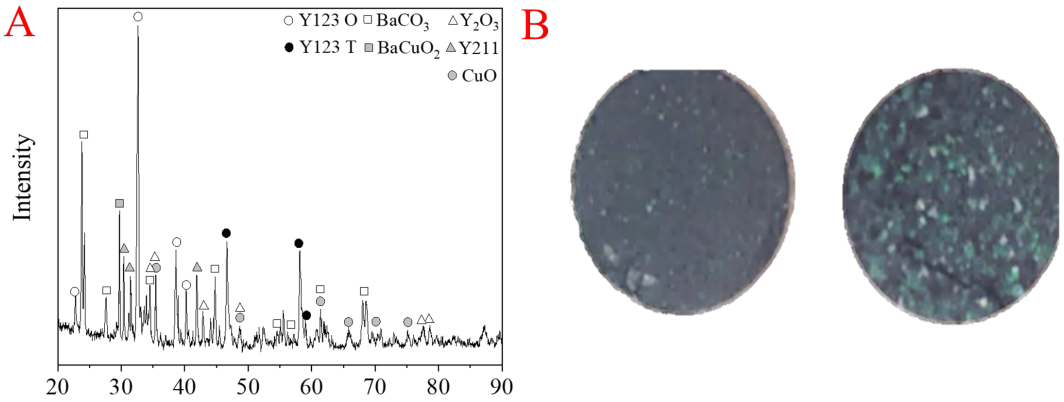


Figure 3.3: A - XRD pattern of sample with Y211, B - Examples of samples without and with Y211 phase.

The XRD analysis evidences that it is easier to obtain pure YBCO with the B mixture, or, contrary to what Abd-Ghani et al.[39] mentioned, in the furnace used in our case, that the temperature needed to obtain YBCO starting from BaO is not 900 °C, but 950 °C. The presence of YBCO 211 can be further reverted to YBCO 123 as suggested by Licci et al.[44] and the presence of the precursors could be solved by using a mixer system that allows a better homogenization of the powders, for instance, by using a mortar instead of a coffee grinder. The pure orthorhombic structure was not achieved, however, this could be solved with oxygenation studies during the sintering process or with a prolonged time at 950 °C as suggested by Mendes et al.[10].
Overall, it is possible to conclude that, to attain YBCO 123, both 900 °C and 950 °C for mixture B (with BaO) can be used, but for mixture A (with $BaCO_3$) only 950 °C should be used.
Different heating curves were tested to check which one would be the best option for the YBCO synthesis. Different ovens were also used to know the reproducibility and its influence in the final product. These different treatments are mentioned in the Methods and Materials chapter and appear in the Methods section of the Appendix chapter. The YBCO could be attained for all treatments except for NFP (heating treatment for 6 hours plus cooling). The preferable treatment should be NFN as it consumes less energy and therefore the production cost can be reduced but it was seen that NFA (heating treatment for 30 hours plus cooling) seems to produce YBCO of higher quality. From the tests performed, the different ovens did not influence the final YBCO characteristics, but the heat treatment should be optimized. Therefore, before the sintering process, it would be useful to know the spatial temperature profile of the furnace to guarantee that the samples are placed inside the furnace where the temperature is the required one.
Electric conductivity measurements were made between two faces of coin shaped samples and were used to test if there was a relation between the temperature and heating treatment (sintering time) with the material's conductivity.
Table 3.1 shows the samples that were tested, with their sintering temperatures (900 °C and 950 °C) and heating treatment (NFN and NFA), as well as with the contacts used (Cu tape or Cu wires). The name of the samples can also be seen, O is used for synthesized powders, M for the milled powders and the number represents the order in which they were made.

Table 3.1: Effect of the heating treatment used, temperature and contacts on the material's conductivity.

| Sample | Temperature/ °C | Heating Treatment | Contacts | Conductivity/ (S/m) |
|---|---|---|---|---|
| O31 | 900 | NFN | tape | 1.380 |
| O33 | 900 | NFA | tape | 3.090 |
| O151 | 900 | NFA | wire | 0.246 |
| MO1 | 950 | NFA | wire | 0.044 |

Comparing samples measured with Cu tape for the NFN or NFA treatment, the results show a dispersion of values within one order of magnitude. The same dispersion of values can be seen for samples measured with copper wires. When comparing the values obtained with the Cu tape with the Cu wire, they seem consistently higher. Regarding the influence of temperature, the results seem to indicate that samples sintered at higher temperature have lower conductivity. For the treatment, the results seem to indicate that the NFA treatment allows for higher conductivity values.
From these measurements it is not possible to conclude if the furnace or sintering temperature has a remarkable influence on the sample's conductivity, as the method used relies primarily on the electric contacts used.

### 3.1.2 Influence of the Milling Time

As referred previously the precursors homogeneity may play an important role in the YBCO 123 phase uniformity in sintered powders. This was investigated by changing the milling time and analyzing its impact in the powder average size, thus, the material was milled for 10, 30, 60 and 180 minutes. According to literature, the best powder's size is below 0.4 µm [14]. The particle size distribution is shown on the histograms included in the SEM images of Figure 3.4 A to D.

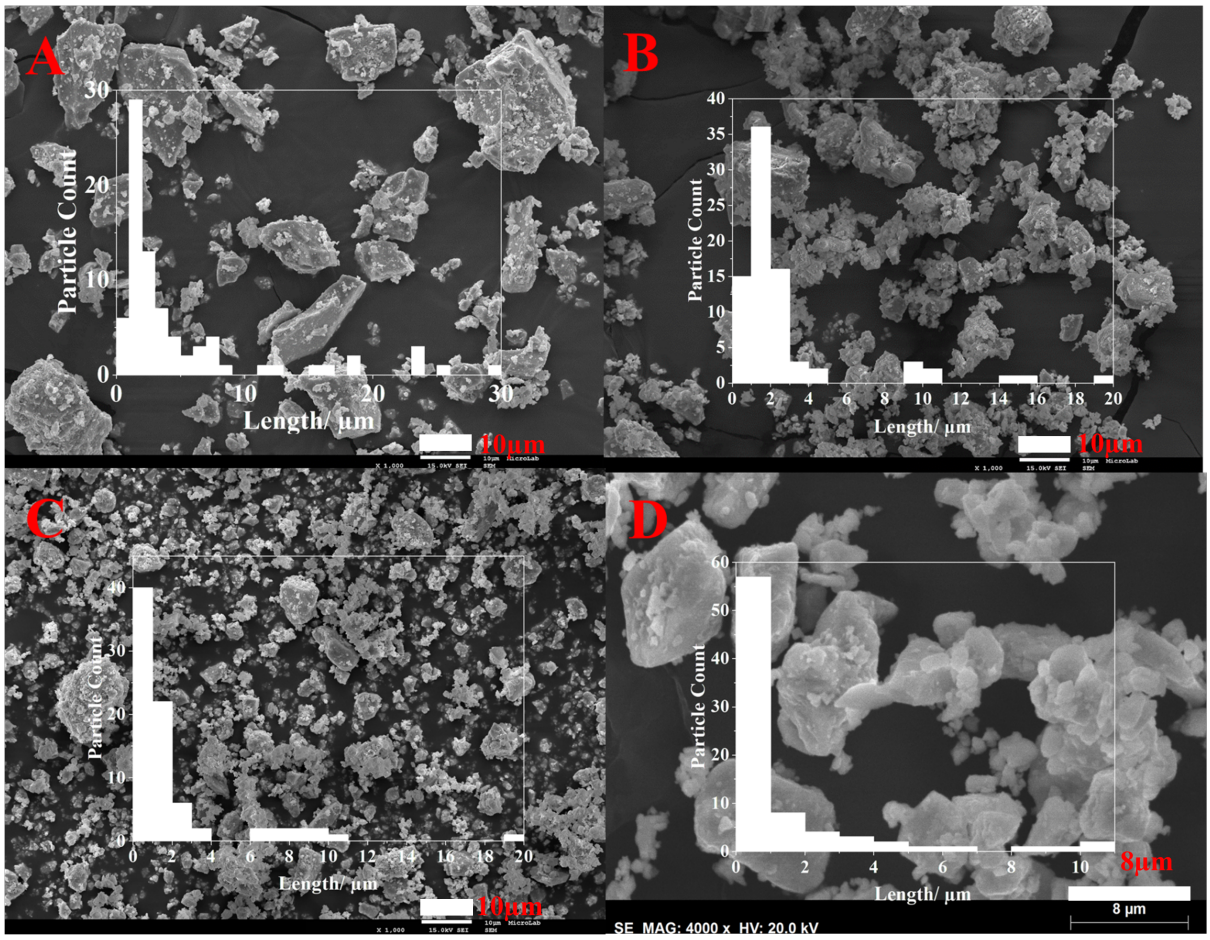


Figure 3.4: SEM images of milled powder for A - 10 minutes (scale 10 µm), B - 30 minutes (scale 10 µm), C - 60 minutes (scale 10 µm), D - 180 minutes (scale 8 µm).

The particles' size distribution is predominantly bellow 10 µm, but clearly narrows down to 2 µm as the milling time increases, proving that to obtain low particle's sizes, milling time over 180 minutes at 500rpm is required. Eventually, the milling time could also be tested but for this work it was not possible to change that parameter. The histogram of Figure 3.5 compares the number of particles inferior to 1 µm and 0.4 µm of the milling time.

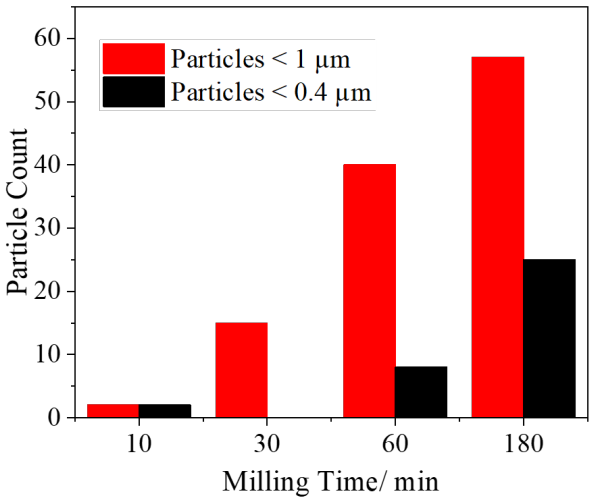


Figure 3.5: Particle count comparison below 1 and 0.4 µm.

The absence of particles below 0.4 µm for 30 minutes may be due to only measuring 80 randomly selected particles. Figure 3.5 clearly shows that, for the selected particles, the higher the milling time is, the smaller the particle and the higher the number of particles smaller than the target size is. It would be interesting to continue to investigate higher milling's times to have the majority of the selected particles smaller than the target size, however, this is a time and energy consuming process, and therefore it must be balanced in terms of properties gain against the energy and time consumption as it impacts the cost of the final product.

### 3.1.3 Influence of the Mixture Used

Magnetization versus Temperature graphs were made to attain the material's $T_C$ and to see the mixture's influence on its vale. The graph is present in Figure 3.6. Zero field cooling (ZFC) and field cooling (FC) were both measured to attain the Meissner signal. ZFC was measured by cooling the sample in zero applied fields and FC by cooling the sample with application of magnetic field.

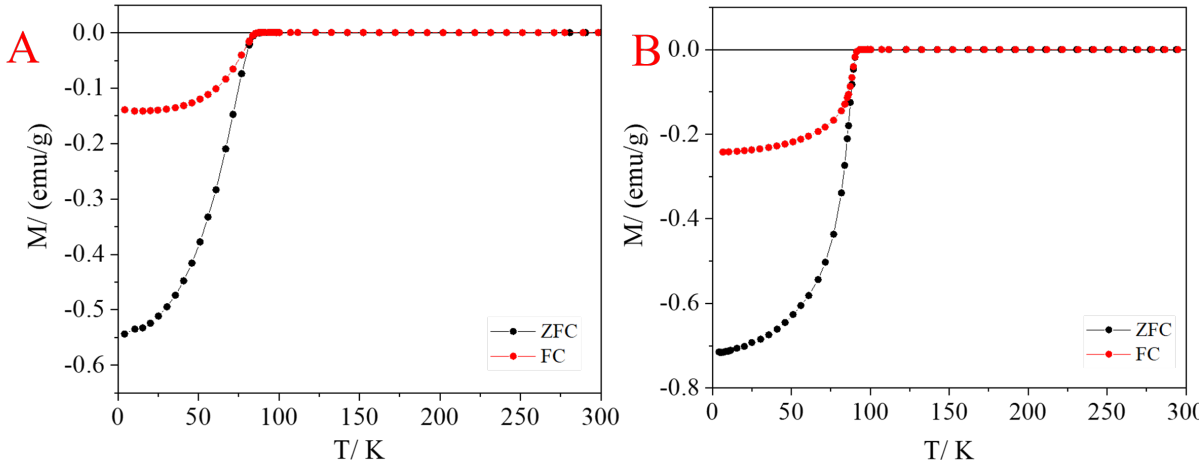


Figure 3.6: Magnetization vs Temperature for A - mixture with $BaCO_3$ and B - mixture with BaO.

The $T_C$ obtained for A was 87K and for B was 91K which is similar to the expected value for YBCO.

Then, values of magnetization versus magnetic field strength were obtained to get the material's $J_C$. To obtain that value it is used the extended Bean critical state model that can be seen below in Equation 3.1.

$$Jc = \frac{20\Delta M}{a(1 - \frac{a}{3b})} \tag{3.1}$$

In the formula, $\Delta M$ represents the width of the magnetization hysteresis loop and a and b (a<b) are the cross section dimensions perpendicular to the applied field. The values used can be seen in Table A.11 present in the Bean Critical State Model Values section of the Appendix chapter. The graphs of magnetization versus magnetic field strength can be seen in Figure 3.7. By using the necessary information from the graph and applying the Bean critical state model it was possible to obtain the values that can be seen in Table 3.2

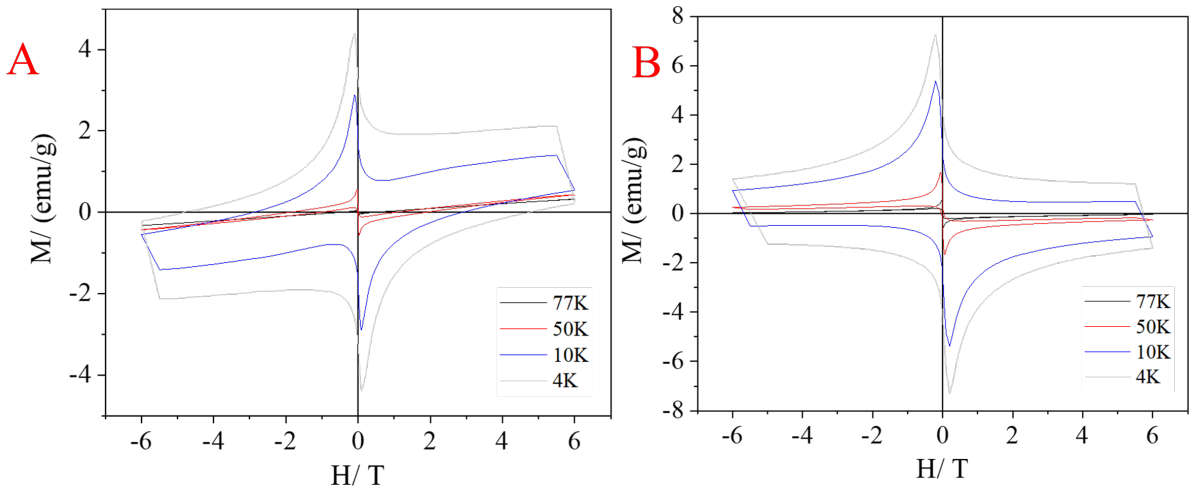


Figure 3.7: Magnetization vs magnetic field strength for A - mixture with $BaCO_3$ and B - mixture with BaO.

Table 3.2: $J_C$ dependence on temperature and mixture (A with $BaCO_3$ and B with BaO).

| | $J_C$ | |
|---|---|---|
| Temperature/ K | Mixture A | Mixture B |
| 77 | 3.90 | 6.91 |
| 50 | 6.74 | 20.08 |
| 10 | 34.66 | 64.67 |
| 4 | 52.79 | 87.64 |

As can be seen in Table 3.2, it seems that mixture B allows for higher $J_C$ values. This could be due to the fact that the temperature used was the one suggested by Abd-Ghani et al.[39] for mixtures made with BaO.
Figure 3.8 shows the graphs that correlate $J_C$ with the magnetic field applied. In this graphs it is possible to obtain the maximum $J_C$ value, and the corresponding magnetic field value, as well as the $J_C$ value when there is no field applied. Those results can be seen in Table 3.3.

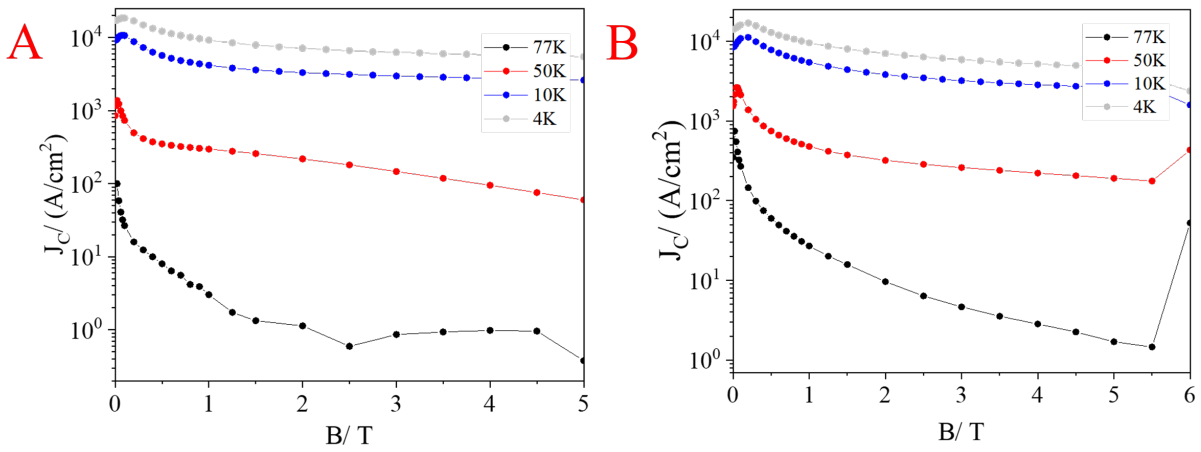


Figure 3.8: Critical current density vs magnetic field for A - mixture with $BaCO_3$ and B - mixture with BaO.

Table 3.3: $J_C$ max results and $J_C$ for when B=0 for mixture A and mixture B.

| | A Mixture | | | B Mixture | | |
|---|---|---|---|---|---|---|
| Temperature/ K | $J_C$ max/ (A/cm$^2$) | B value for max $J_C$/ T | $J_C$ when B=0/ (A/cm$^2$) | $J_C$ max (A/cm$^2$) | B value for max $J_C$/ T | $J_C$ when B=0 (A/cm$^2$) |
| 77 | $9.91x10^1$ | 0.00 | $9.91x10^1$ | $7.44x10^2$ | 0.02 | $3.51x10^2$ |
| 50 | $1.38x10^3$ | 0.02 | $8.55Ex10^2$ | $2.62x10^3$ | 0.04 | $1.54x10^3$ |
| 10 | $1.08x10^4$ | 0.08 | $9.16x10^3$ | $1.12x10^4$ | 0.20 | $8.45x10^3$ |
| 4 | $1.85x10^4$ | 0.10 | $1.72x10^4$ | $1.70x10^4$ | 0.20 | $1.42x10^4$ |

With these results it is possible to observe, as was expected, that the $J_C$ values decrease while the temperature increases. It is also possible to conclude that B mixture allows for higher magnetic field and $J_C$ values when comparing with the A mixture.

### 3.1.4 Magnetic Levitation of YBCO Pellets

Figure 3.9 shows the levitation of one of the samples. In this particular image it is possible to see a sample that was not stable while levitating due to its irregular shape.

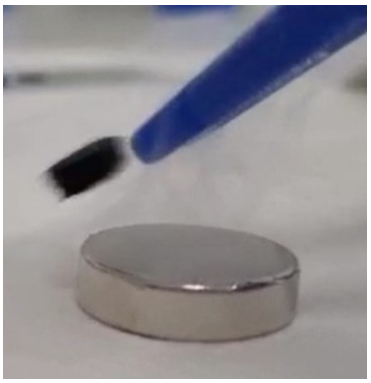

Figure 3.9: Demonstration of the samples levitation.

From obtained experiments, that can be observed in the section Levitation Performance of the Appendix chapter, it was concluded that YBCO samples do levitate independently of the furnace

used and type of precursors, for example mixture A - O8, O26 and mixture B O13,O23. However it is important to mention that none of those samples possessed YBCO 211 characteristic green phase, and the samples which contained the green phase did not levitate. All the samples that had a green phase did not levitate.
The milled samples (MO1, MO3, MO4) also levitated, but for MO1 the green phase was detected meaning that it could not be enough to influence the overall magnetic field of the samples. About 75% of the samples not presenting green phase did levitate. Although there is a possible relation between green phase YBCO 211 and the non-superconducting properties, the presence of tetragonal or a mix of tetragonal and orthorhombic phases can be also the origin of the behavior. However, from the results, this is not conclusive since some samples with detected orthorhombic structure did not levitate.
A complete table with the samples' details, such as heat treatment, presence of green phase, structure, mix/original powder used, and their levitation performance can be seen in Table A.12 in The Levitation Performance section of the Appendix chapter.

## 3.2 3D Printing and Recycling

The attempts made for 3D printing YBCO using sintered powders or the precursors' mixture and their recyclability are shown in this section. For 3D printing, different binders and solvents were tested to obtain a paste that was able to be extruded and printed. Concerning recycling tests, the work performed aimed to understand the viability of recycling already processed samples and recover its materials for the printing of new samples with similar properties. This would show that YBCO powders that were used for printing or were used in unsuccessful parts, could be recovered and used for new pastes and printing pieces.

### 3.2.1 3D Printing

The printing process requires the use of a suitable paste made with the YBCO powders and an adequate binder, being that, it depends on the powder's type. In case of YBCO water-based, binders must be avoided due to possible reaction with powders, making a highly basic paste. Another key aspect is the extrudability, where viscosity and rheological aspects are important. Without access to a rheometer, the study was made by trial and error. Thus, several pastes were tested and evaluated by their extrudability, printability and levitation. Only pastes that were extrudable by a syringe, printable and that retained the printed structure, will be shown in this section. Printing process parameters were adjusted, such as drying time, the sticking between layers, the form stability along the printing process, etc. For this study, simple design pieces were tested such as the ones of Figure 3.10.

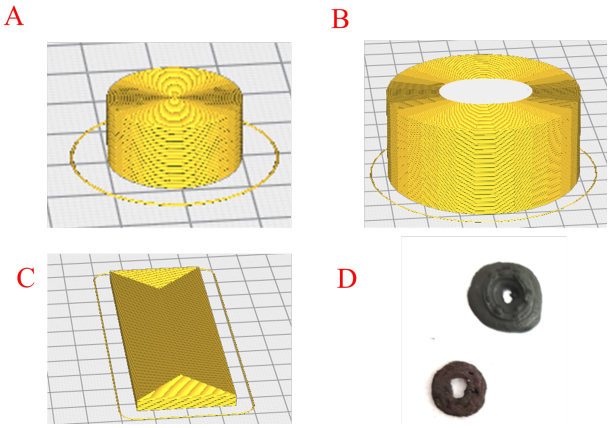


Figure 3.10: A, B, C - examples of the designs chosen to print, D - example of the samples printed.

Pastes made with polystyrene (PS), xylene, dichloromethane and polysorbate 80 were tested. These samples were made with YBCO precursors and not with YBCO powder. The pastes were easier to extrude and print when compared to pastes that used YBCO powder and were tested with both mixtures.
Pastes made with dimethylformamide (DMF), xylene and PS were also tested. Although they had some issues at first, after a simple optimization regarding its viscosity, it was possible to print synthesized YBCO with good resolution.
Some of the problems found for most of the pastes that were not extrudable were, quick solidification, using an excessive amount of powder material, reaction with one of the precursors, or phase separation. Another experimental observation was that printed pieces with powder that did not levitate, still did not levitate even after the sintering process. This could mean that the thermal treatment did not lead to the formation of the orthorhombic phase, nor removed the YBCO 211 phase, which seems to affect the superconductor properties. The complete list

of tested pastes can be seen in Table A.17 and Table A.18 on the 3D Printing section of the Appendix chapter.

### 3.2.2 Recycling

The recycling studies aimed to understand the possibility to recover either powders or sintered pieces of YBCO. The samples that were printed and others from the previous work of Mendes et al.[7] were recycled by using a two-step process: first annealing at 900 °C and then milling for 180 minutes at 500rpm.
The recycled powders were analyzed by XRD, electrical measurements, SQUID and levitation tests.
Electrical measurements were done to see if the recycling process and the milling time affected the material's conductivity. Table 3.4 shows the samples measured as well as their original powder, the milling time used, the contacts and the original powder's conductivity.

Table 3.4: Effect of the original powder, milling time and contacts on the material's conductivity and comparison between its original value and the value after the recycling process.

| Sample | Original Powder | Milling Time/ min | Contacts | Original Conductivity (S/m) | Conductivity (S/m) |
|---|---|---|---|---|---|
| O28 2 | O28 1 | 180 | tape | 0.74 | 0.93 |
| MR7 | Mendes' | 180 | tape | - | 12.60 |
| MR2 | Mendes' | 10 | wire | - | 0.43 |

Regarding the milling time, it is possible to see that 180 minutes seem to allow for better conductivity. However, it is important to note that, as was seen before in the Influence of Temperature and Time section, the sample that possessed the lowest conductivity value was the one measured with Cu wires. After the recycling process the conductivity remained with similar but slightly better values as its original powder. Mendes' recycled pieces seemed to have higher conductivities, for the same conditions, which could be explained by the original powders' superior superconductor properties (such as the ability to levitate), possibly due to longer sintering times at 950 °C.
Levitation tests were necessary in order to know if the samples, after the recycling process, exhibited superconducting properties when the temperature was below $T_C$. For that, the conditions mentioned in the Materials and Methods chapter were used. The levitation performance table can be seen in Table A.13 of the Levitation Performance section of the Appendix Chapter and it correlates the original powder used, heat treatment, the presence of green phase and the material's structure with its levitation.
With these results, it is important to mention that the pieces after the recycling process did not appear to have the presence of YBCO 211 but it would be interesting to know if it was present before the recycling process. These results also seem to agree with the conclusion that the YBCO 211 presence suppresses the levitation.
SEM analysis of the recycled powders are shown in Figure 3.11. The analysis of particle average size was made as explained before in the Influence of the Milling Time subsection.

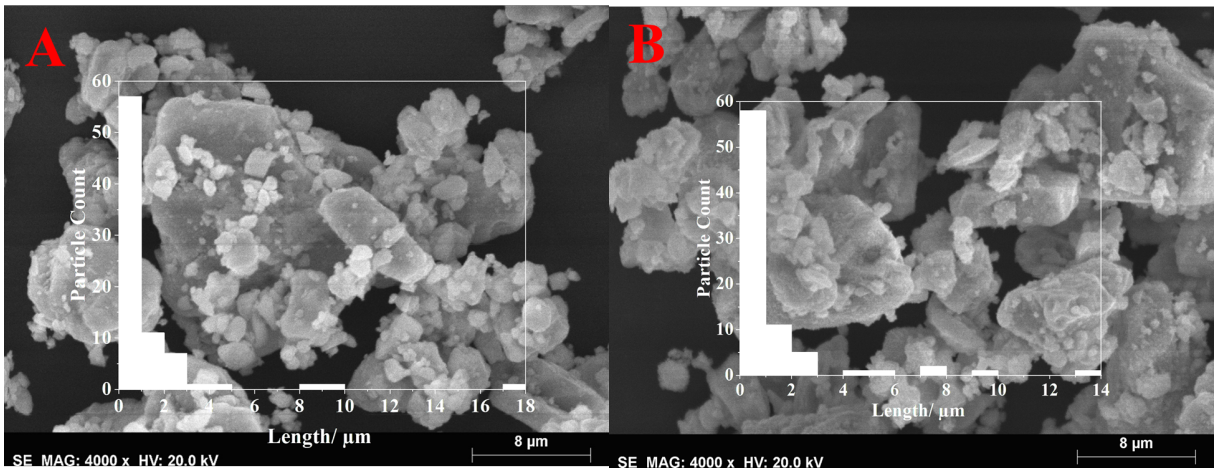


Figure 3.11: SEM images and histogram for samples A - before the recycling cycle, B - after the recycling cycle.

After the recycling process, the particle size distribution was similar to the one obtained before the recycling process as can be seen in Figure 3.11. XRD analysis also shows similarity between the samples. The XRD spectra are shown in Figure 3.12 A and B.

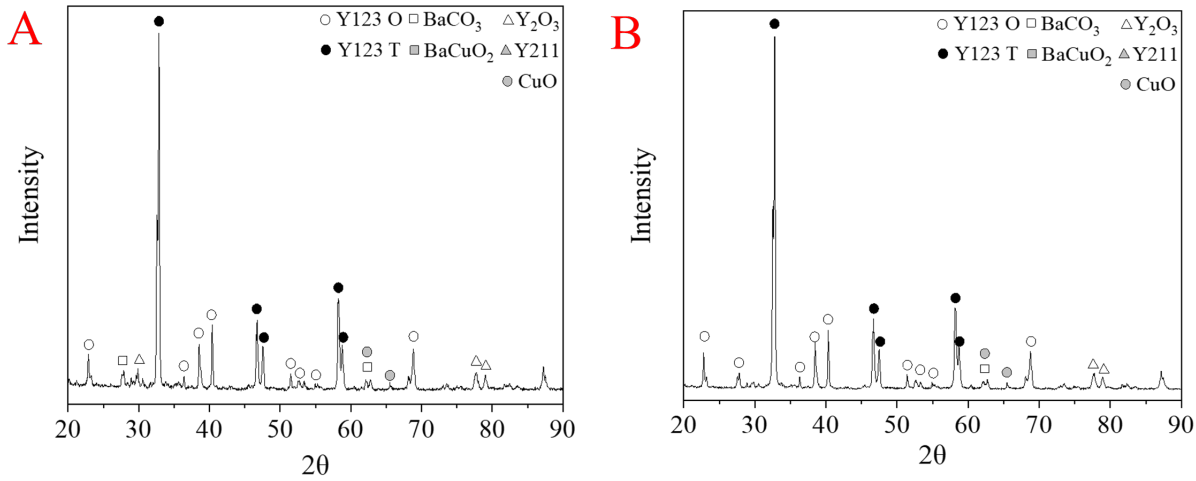


Figure 3.12: XRD pattern for samples A - before the recycling cycle, B - after the recycling cycle.

The YBCO 123 is the main phase and the relation between peaks remains almost the same. Regarding the phase structure, the sample from before the cycle shows a tetragonal phase with the peaks at 33°, 47°, 48°, 58° and 59° and an orthorhombic phase given by the peaks at 36°, 39° and 40°. The sample from after the cycle seams to retain the same structure of the original powder, meaning that the recycling process did not alter the material structure. This suggests that it is viable to do multiple recycling cycles in cases where it is wanted to retain the material original structure.
The 3D printing of recycled powders was tested. Pastes made with oleic acid, oleylamine, ammonium solution, distilled water and sodium dodecyl sulphate (SDS) were tested. This paste demonstrated a tendency for the formation of clusters when in contact with YBCO, making it hard to extrude and print. However, even with pastes that were able to be extruded, the piece's resolution was not good enough. Pastes made with DMF, xylene and PS were again tested, but this time with recycled powders instead of synthesized ones. As it was seen with the synthesized powders, this paste was also able to be extruded and printed with great quality with recycled

powders.
The pastes that were not extrudable or printable appeared to have the same issues as the pastes made with the non-recycled powders. The complete list can be seen in Table A.17 and Table A.18 of the 3D Printing section of the Appendix chapter.
Levitation tests revealed that recycling was possible with pieces that were printed in Mendes' thesis [7]. It was also possible to see that the recycling process did not change the ability or inability of the original powder to make samples that levitate. The complete levitation performance table can be seen in Table A.12 of section Levitation Performance of the Appendix chapter.
In Figure 3.13 it is possible to observe the graphs of magnetization versus temperature, magnetization versus magnetic field strength and critical current density versus magnetic field.

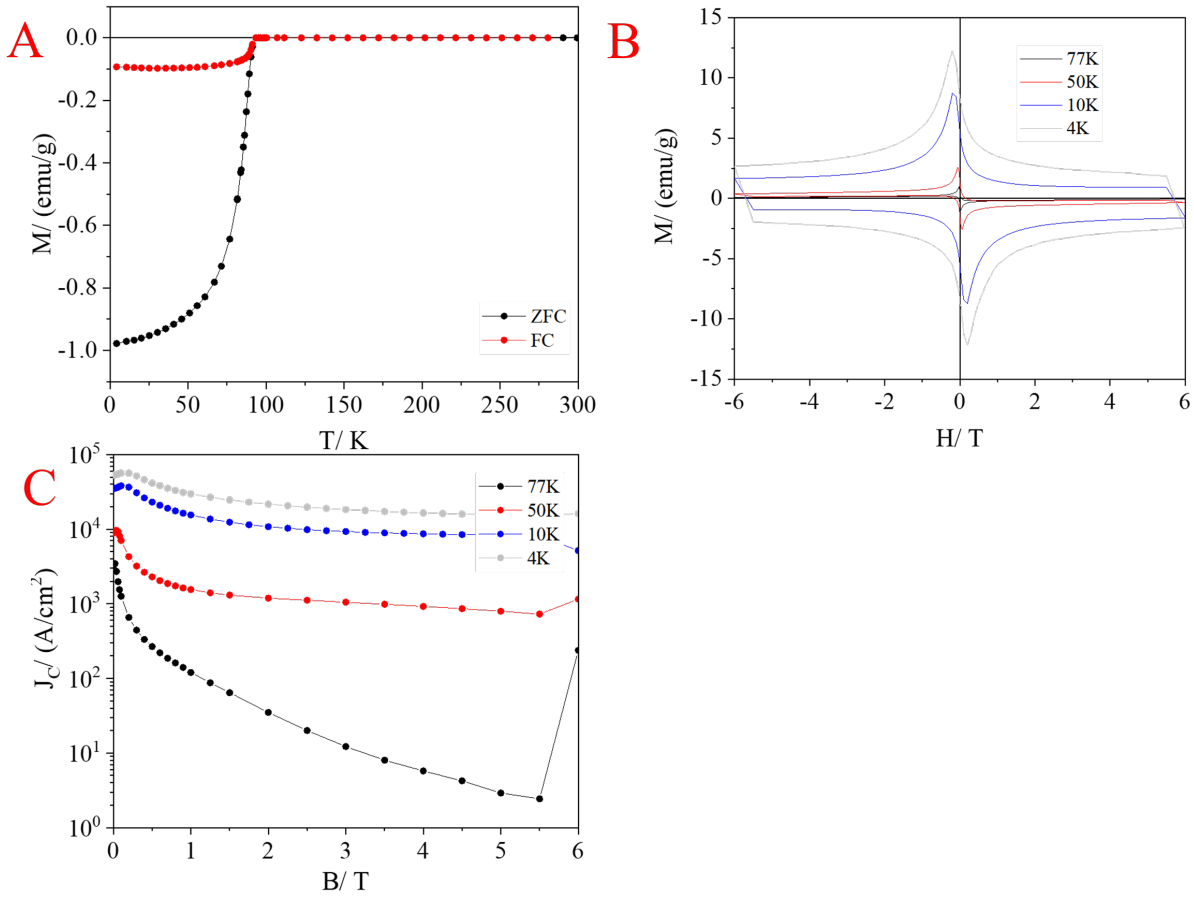


Figure 3.13: A- magnetization versus temperature, B - magnetization versus magnetic field strength and C - critical current density versus magnetic field.

In Figure 3.13 A it is possible to attain the $T_C$ value, which is 93K. This value is similar to the expected value for YBCO. With the data obtained from Figure 3.13 B and the values present in Table A.11 of the Bean Critical State Model Values section of the Appendix chapter it was possible to obtain the results presented in Table 3.5. This data was obtained by the Bean critical state model as it was mentioned in the Influence of the Mixture Used subsection of the Synthesis of YBCO section of the Results chapter.

Table 3.5: $J_C$ of recycled YBCO dependence on the temperature used.

| Temperature/ K | $J_C$ |
|---|---|
| 77 | 12.28 |
| 50 | 46.22 |
| 10 | 154.67 |
| 4 | 216.89 |

The data obtained shows that, as it was predicted, that the $J_C$ increased with the temperature decrease. It is also possible to see that the results obtained for the recycled piece have higher values than the results obtained for synthesized samples. This could be due to the superior properties of the original pieces that were recycled, when compared to the synthesized pieces. With Figure 3.13 C it is possible to obtain Table 3.6 by choosing the highest value of $J_C$ and the value of $J_C$ when B=0.

Table 3.6: $J_C$ max results and $J_C$ for when B=0.

| Temperature/ K | $J_C$ max/ (A/cm$^2$) | B value for max $J_C$/ T | $J_C$ when B=0/ (A/cm$^2$) |
|---|---|---|---|
| 77 | 3.45x10$^3$ | 0.02 | 3.07x10$^3$ |
| 50 | 9.63x10$^3$ | 0.04 | 8.86x10$^3$ |
| 10 | 3.81x10$^4$ | 0.10 | 3.49x10$^4$ |
| 4 | 5.64x10$^4$ | 0.10 | 5.37x10$^4$ |

This data also shows higher $J_C$ when compared to the synthesized samples but with magnetic field's values lower for the maximum $J_C$. Once again, this could be due to the superior superconductor properties in the original sample. Table 3.5 and Table 3.6 prove that after the recycling process, the superconductor properties do not cease to exist due to the recycling process.

## 3.3 Doping

As an attempt to increase the critical temperature of YBCO, doping was tried with graphene, iron(III) and calcium(II). Raman spectroscopy, XRD, electric measurements and levitation tests were analyzed for some of the doped samples to understand the doping effect on the YBCO samples.

### 3.3.1 Calcium(II) Doped

The XRD diffractogram and the Raman spectra of samples doped with $CaCl_2$ show the influence of doping in the material characteristics. For the XRD it was chosen the samples with the highest doping content to have the highest probability of finding doped samples. For the Raman spectroscopy it was chosen the most and the least doped samples to see the variation of the peaks, according to different doping concentrations. The measurements points for sample Ca with 0.1 wt% and 0.3 wt% can be seen in Figure A.4 of the Raman Photos section in the Appendix chapter.

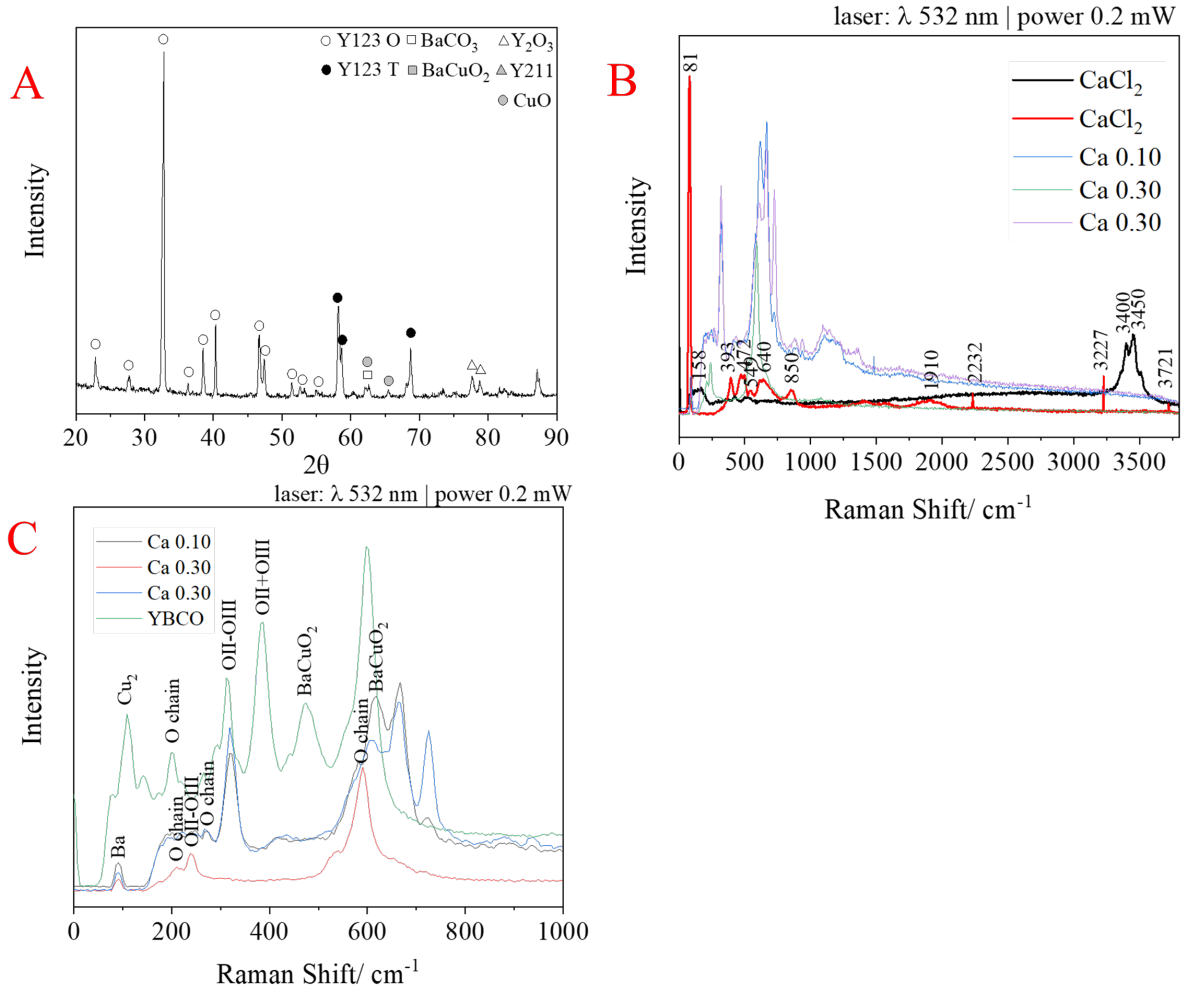


Figure 3.14: A - XRD pattern of calcium(II) doped YBCO, B - Raman spectrum of calcium(II) doped YBCO, C - Section of the Raman spectrum of pure and calcium(II) doped YBCO.

The XRD diffractogram of YBCO 123 with 0.3 wt% of Ca(II) is similar to YBCO 123, where the orthorhombic phase is predominant (peaks 33 °, 36°, 38° and 40°). The tetragonal phase is also present at 58°, 59° and 69°. No vestiges of Ca were present which is expected due to its low concentration. Due to that, Raman spectroscopy was performed to try to detect Ca.

There are known and common vibration modes of the orthorhombic structure such as Ba at 110 $cm^{-1}$, $Cu_2$ between 140 and 150 $cm^{-1}$ and the out-of-phase, centro-symmetric mode OII-OIII at 340 $cm^{-1}$, due to the atoms of the Cu-O plates that carry the supercurrent, OII+OIII at 450 $cm^{-1}$ and OIV between 475 and 500 $cm^{-1}$ [45]. There are also some undesirable peaks, such as $BaCuO_2$ around 430 $cm^{-1}$ that is due to the reaction between precursors [46]. The O chain peak correspond to defect-induced Raman peaks due to oxygen chains not being fully occupied, which could lead to the presence of the tetragonal phase if the O proportion is below 6.4, or could lead to an higher carrier's concentration that could raise the $J_C$ value [42],[47].
The Raman spectra in Figure 3.14 B compares the Raman spectra of samples of $CaCl_2$ and samples with 0.05 and 0.3 wt% of Ca(II). It is possible to observe that the samples do not show any of the Raman peaks related to $CaCl_2$ which could be caused by an unsuccessful doping process, due to the dopant not being in the surface of the sample or due to the transformation of $CaCl_2$ in others Ca compounds at high temperature. In Figure 3.14 C it is possible to see some peaks characteristic of the YBCO such as Ba, OII-OIII as well as O chain and $BaCuO_2$ peak. When comparing with the spectra of the non-doped YBCO it is possible to see some common peaks (Ba, the last O chain peak and the OII-OIII peak ) but the majority of the non-doped peaks were not present. Figure 3.14 B and Figure 3.14 C show different spectrums for the same components (Ca 0.30 and $CaCl_2$) due to them not being homogeneous and possessing spectrums with different peaks.
Electric conductivity measurements were performed to check the relation between doping percentage and the sample's conductivity. For this, it was used four Ca doped YBCO samples with NFN treatment at 900 °C, with Cu tape for contacts. In Table 3.7 it is possible to see the results.

Table 3.7: Relation between doping content and conductivity in Ca(II) doped YBCO.

| Sample | Doping Content | Conductivity (S/m) |
|---|---|---|
| CaO22 | 0.10 | 1.11 |
| CaO23 | 0.15 | 0.17 |
| CaO24 | 0.20 | 1.05 |
| CaO25 | 0.30 | 0.36 |

With the information presented above, it is possible to see that there seems to be a relation between doping and the conductivity value, with a decreasing in the conductivity with the increase of the doping content. This goes according to what Mohan et al.[48] reported. In the 0.15 wt% doping content point value seems to have occurred some kind of mistake since it does not seem to follow the correlation of the other values.
Regarding the levitation tests, the conditions were equal to the tests made with non-doped samples. In those tests it was possible to see that none of the doped samples did levitate, probably due to the presence of the Y211 phase and the tetragonal structure of the material, or due to the short sintering phase. The levitation performance table can be seen in Table A.14 in the Levitation Performance section of the Appendix chapter

### 3.3.2 Graphene Doped

XRD diffractogram and Raman spectra were obtained to know the influence of graphene doping on the material's characteristics. For the XRD it was selected the sample with the highest doping content to make sure that it would be possible to find doping content in the sample. For the Raman it was selected the samples with the highest and the lowest doping content to see differences in the materials present, according to the different doping contents. The regions chosen for the Raman spectroscopy can be seen in Figure A.5 or the Raman Photos section in the Appendix chapter.

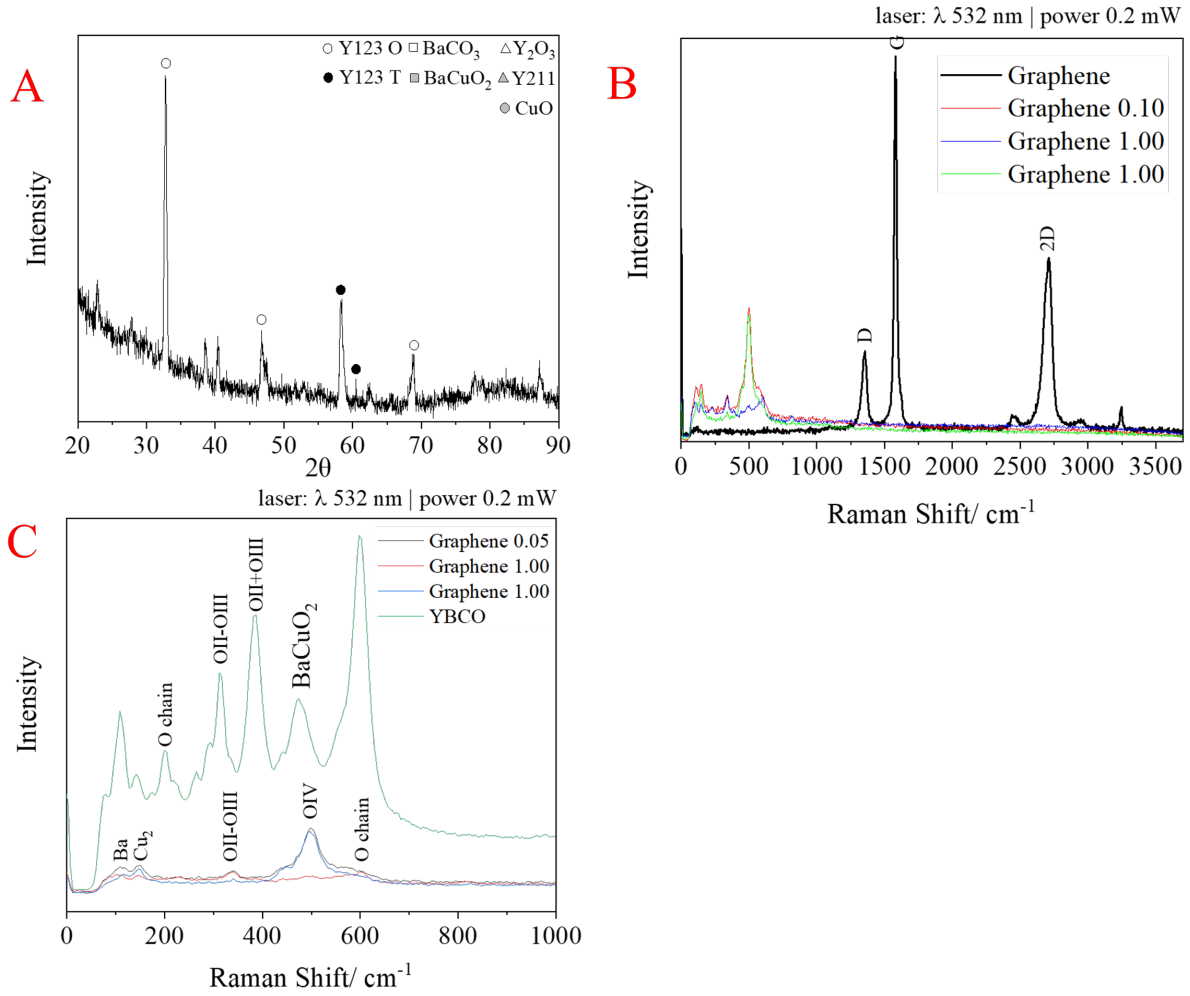


Figure 3.15: A - XRD pattern of graphene doped YBCO, B - Raman spectrum of graphene doped YBCO, C - Section of the Raman spectrum of pure and graphene doped YBCO.

The presence of YBCO 123 orthorhombic phase is present and predominant as revealed by the main peaks 33° and 47°. Tetragonal structure phase is also present due to the peaks 58° and 60°. Regarding doping, no peaks related to graphene or graphite were observed. The XRD pattern peak of the graphene is a band around 26° and coincide with graphite peak, except for the intensity which is much lower [49]. Due to the high intensity of YBCO peaks and the low content of graphene in the powder mixture it was expected to be undetected through XRD. Therefore Raman analysis was performed.
When looking at Figure 3.15 B the graphene peaks G, D and 2D are present. This peaks are due to out of plane vibrations due to structural defects, due to plane vibrations of sp2 carbon atoms and due to second order two phonon process dependent on the excitation laser, respectively [35],[50]. Regarding the raman spectrum, when looking at Figure 3.15 B it is possible to

see that the sample did not have any trace of the supposed graphene. This could be due to an unsuccessful doping or that the Raman should not be used for pellets due to the fact that it only sees the surface. When looking at Figure 3.15 C, it is possible to see some peaks typical of YBCO such as Ba, $Cu_2$, OII-OIII and OIV, meaning that some YBCO was produced. The peak characteristic of the O chains is also present, meaning that there is not enough oxygen in the structure. When comparing the doped samples' Raman spectra with the non doped samples, it is possible to see that most of the non-doped YBCO peaks are present in the doped samples, with the exception of the OII-OIII peak.
To attain the relation between conductivity and doping content, electric measurements were made. For this, graphene doped YBCO samples with the same heating treatment (NFN), sintering temperature (900 °C) and contact (Cu tape) were chosen. In Table 3.8 it is possible to see the conductivity and the doping content values.

Table 3.8: Relation between doping content and conductivity in graphene doped YBCO.

| Sample | Doping Content | Conductivity (S/m) |
|---|---|---|
| GO21 | 0.10 | 1.09 |
| GO23 | 0.70 | 2.40 |
| GO24 | 1.00 | 1.17 |

With these results it is possible to see that, apparently there is a maximum in the 0.7 wt% of graphene doping, meaning that value could be the best one for applications that require higher conductivity values. Those results are according to what Gaffoor et al.[35] concluded.
Regarding the levitation tests, the conditions were equal to the tests made with non-doped samples and it was possible to observe that none of the doped samples did levitate, probably due to the presence of the Y211 phase and the structure of the material. The levitation performance table can be seen in Table A.15 in the Levitation Performance section of the Appendix chapter.

### 3.3.3 Iron(III) Doped

XRD and Raman spectroscopy were made in order to attain the influence of the $Fe_2O_3$ doping in YBCO. For both the XRD and the Raman spectroscopy, the sample with the highest doping content was chosen to be sure that it was possible to find doping content in the sample. The sample's region chosen for the Raman spectroscopy can be seen in Figure A.6 of the Raman Photos section in the Appendix chapter.

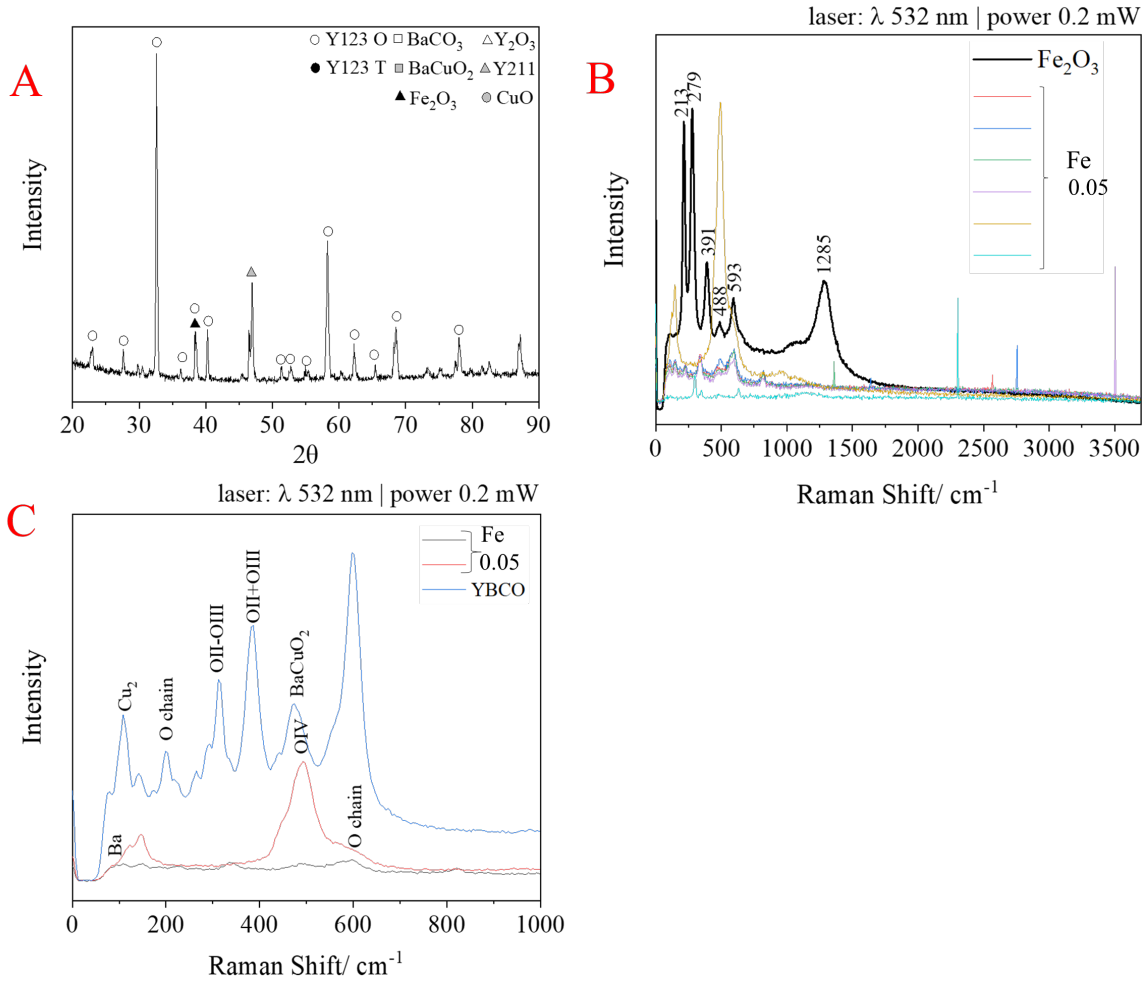


Figure 3.16: A - XRD pattern of iron(III) doped YBCO, B - Raman spectrum of iron(III) doped YBCO, C - Section of the Raman spectrum of pure and iron(III) doped YBCO.

The presence of YBCO 123 orthorhombic phase is present and predominant as revealed by the main peaks 33°, 36°, 38°, 40° and 68°. Regarding doping, 37° corresponds to a peak of $Fe_2O_3$, meaning that some doping may have been possible. It is also possible to observe a peak at 47° that corresponds to YBCO 211.
Regarding the Raman spectrum that can be seen in Figure 3.16 B, it is possible to see that there seems to be some peaks in common between the doped samples and $Fe_2O_3$ and that the samples are highly non-homogeneous. It is also important to note that, due to its heterogeneity, the Raman spectra are not the same for the same sample, explaining the necessity for multiple Fe 0.05 wt% spectra. When looking at Figure 3.16 C, it is possible to see the presence of some of the YBCO's peaks such as Ba, $Cu_2$, OII-OIII and OIV as well as the O chain. When comparing the doped YBCO with the non-doped it is possible to see that the doped does not have the majority of the virgin YBCO peaks.
In order to correlate conductivity and the doping content, electric measurements on the doped

samples were made. For this, samples with the same sintering temperature (900 °C), heating treatment (NFN) and contact (Cu tape) were chosen. The results can be seen in Table 3.9.

Table 3.9: Relation between doping content and conductivity in Fe(III) doped YBCO.

| Sample | Doping Content | Conductivity (S/m) |
|---|---|---|
| FeO21 | 0.01 | 1.00 |
| FeO22 | 0.02 | 0.84 |
| FeO23 | 0.03 | 0.01 |
| FeO24 | 0.04 | 1.84 |
| FeO25 | 0.05 | 0.70 |

From the results, it does not seem to exist a correlation between doping and the conductivity value. This could be due to the fact that the doping values were too close to one another. However the results seem to go according to the order that Abd-Ghani et al.[39] suggested for 0.04 and 0.01 wt%.
Regarding the levitation tests, the conditions were equal to the tests made with non-doped samples and none of the doped samples levitated, probably due to the presence of the Y211 phase and the structure of the material. It is also possible that the presence of the dopant affected the superconductor properties. The results of the levitation performance can be seen in Table A.16 of the Levitation Performance section of the Appendix chapter.

# Conclusion

The main objectives of the present work were: 1-synthesis of YBCO, 2-3D printing of YBCO pastes, 3-recycling of YBCO, and 4-doping of YBCO with different materials. The conclusions from this work were:

1-The synthesis of YBCO was possible using two different precursors of Ba (BaO and $BaCO_3$). From both was possible to obtain YBCO with superconducting properties that were verified by its levitation in liquid nitrogen over a magnet. However this properties are dependent of sintering temperature, type of furnace, and milling speed and time. It was verified that 900 °C is a suitable sintering temperature to obtain YBCO 123, which showed predominantly orthorrombic phase and some peaks of tetragonal phase. Milling time of 180 minutes is the most adequate to obtain a large number of low particles' size of the sintered powders.
2-The printing of YBCO was also successively done, having achieved a paste of dimethylformamide, xylene and polystyrene that is believed to be a fine candidate for 3D printing and future optimizations.
3-An important aspect of this thesis was to demonstrate that it is possible to recycle YBCO. After the pieces' reprocessing, which included re-sintering, re-milling and re-printing, the results showed that the printed pieces made of recycled YBCO powder had similar or slightly better superconductor properties when compared with the original ones. It was possible to see that the superconductor properties were kept after one cycle. Another important conclusion was that the recycling of materials that previously had not shown good superconductor properties, still kept those properties and there was no improvement with recycling. Regarding 3D printing, it was possible to produce pastes that were deemed of good quality for synthesized and recycled YBCO.
4-The study of doping was performed for calcium(II), iron(III) and graphene. The tested dopants and their respective concentrations did not enhance the superconducting properties as none of the samples levitate in liquid nitrogen. This was a very exploratory and preliminary study which deserves further studies to be more conclusive.

In future studies it will be important to consider the furnace spatial temperature profile to ensure that the required temperature is reached in the furnace or the place where samples are located inside the furnace. This can save time to understand why the same sintering temperature does not lead to the same results of phases and structure. Regarding recycling, more cycles should be studied to know how many cycles the material can endure before losing or deteriorating its superconductive properties. This is an important topic and achievement as the costs of fabrication are high and the possibility of its recycling opens new directions of applications. The topic of doping did not succeed in this study which could be due to the low concentrations used and its probable inability to modify the YBCO's structure. Therefore, other dopant concentrations need to be studied. Samples should also be tested using inductively coupled plasma atomic emission spectroscopy to quantify the doping elements in the final powder. It would be compelling to investigate new possible alloys or doping contents and agents with simulation in order to see how different materials affect the YBCO's structure.

# Bibliography


[1] A. Saxena, *High-Temperature Superconductors*, R. Hull, R. Osgood Jr, J. Parisi, and H. Warlimont, Eds. Springer, **2010**, p. 218.

[2] H. Kamimura, H. Ushio, S. Matsuno, and T. Hamada, *Theory of Copper Oxide Superconductors*. Berlin: Springer, **2005**, p. 192.

[3] R. Huebener P., *Conductors, Semiconductors, Superconductors*, N. Ashby, W. Brantley, M. Fowler, M. Inglis, H. Klose, and H. Sherif, Eds. Tübingen: Springer, **2015**, p. 204.

[4] D. Duan, H. Yu, H. Xie, and T. Cui, "Ab Initio Approach and Its Impact on Superconductivity," *Journal of Superconductivity and Novel Magnetism*, vol. 32, no. 1, pp. 53–60, **2019**, ISSN: 15571947.

[5] O. Jankovský, F. Antončík, T. Hlásek, V. Plecháček, D. Sedmidubský, Š. Huber, M. Lojka, and V. Bartůněk, "Synthesis and properties of YBa2Cu3O7-$\delta$ – Y2Ba4CuWO10.8 superconducting composites," *Journal of the European Ceramic Society*, vol. 38, no. 6, pp. 2541–2546, **2018**.

[6] M. Mueller and H. Polinder, *Electrical drives for direct drive renewable energy systems*, M. Mueller and H. Polinder, Eds. Cambridge: Woodhead Publishing, **2013**, p. 248.

[7] D. Mendes, "Impressão 3D de Materiais Supercondutores," Ph.D. dissertation, Universidade Nova de Lisboa, **2019**.

[8] Laboratory Akimitsu, *Characteristics of Superconductivity!!* [Online]. Available: http://www.okayama-u.ac.jp/user/akimitsu/achievements/study_sc_chara_eng.html (visited on 2021).

[9] A. Rodrigues, *Superconducting magnetic levitated bearings for rotary machines*, **2003**. [Online]. Available: https://slideplayer.com/slide/5225978/ (visited on 2021).

[10] D. Mendes, D. Sousa, A. C. Cerdeira, L. C. Pereira, A. Marques, J. Murta-Pina, A. Pronto, and I. Ferreira, "Low-cost and high-performance 3D printed YBCO superconductors," *Ceramics International*, vol. 47, no. 1, pp. 381–387, **2021**. [Online]. Available: https://doi.org/10.1016/j.ceramint.2020.08.143.

[11] F. Delorme, J. F. Bardeau, C. Harnois, and I. Monot-Laffez, "Evidence of oxygen content heterogeneity in TSMTG YBa2Cu3O7 - $\delta$/Y2BaCuO5 composites by micro-Raman spectrometry," *Physica C: Superconductivity and its Applications*, vol. 468, no. 5, pp. 388–393, **2008**, ISSN: 09214534.

[12] K. Zmorayova, V. Antal, M. Radusovska, S. Piovarci, D. Volochova, and P. Diko, "Microstructure and properties of Y-123/Y-211 bulk superconductors with BaCeO3 and BaO2 addition," *Acta Physica Polonica A*, vol. 126, no. 1, pp. 366–367, **2014**, ISSN: 1898794X.

[13] S. I. Bondarenko, V. P. Koverya, A. V. Krevsun, and S. I. Link, "High-temperature superconductors of the family (RE)Ba2Cu3O7-$\delta$ and their application (Review Article)," *Low Temperature Physics*, vol. 43, no. 10, pp. 1125–1151, **2017**. [Online]. Available: http://dx.doi.org/10.1063/1.5008405.

[14] X. Wei, E. Peng, Y. Xie, J. Xue, J. Wang, and J. Ding, "Extrusion printing of a designed three-dimensional YBa2Cu3O7-x superconductor with milled precursor powder," *Journal of Materials Chemistry C*, vol. 5, no. 13, pp. 3382–3389, **2017**.

[15] M. Izumi and J. Nouden, "Improvement of Critical Current Density and Flux Trapping in Bulk High-Tc Superconductors," *Superconductors: Materials,Properties and Applications*, **2012**, Chapter 4.

[16] S. I. Yoo, H Fujimoto, N Sakai, and M Murakami, "Melt-processed LRE-Ba-Cu-O superconductors and prospects for their applications," vol. 250, pp. 439–448, **1997**.

[17] D. U. Gubser, "Superconducting motors and generators for naval applications," vol. 396, pp. 1192–1195, **2003**.

[18] S Marinel, J Wang, I Monot, M. P. Delamare, and J Provost, "Top-seeding melt texture growth of single-domain superconducting," vol. 147, **1996**.

[19] D. L. Creedon, M. Goryachev, N. Kostylev, T. B. Sercombe, M. E. Tobar, D. L. Creedon, M. Goryachev, N. Kostylev, and T. B. Sercombe, "A 3D printed superconducting aluminium microwave cavity," vol. 032601, pp. 1–5, **2016**.

[20] D Ponnusamy and I Introduction, "Extrusion of superconducting wires of," vol. 4792, no. August 1992, **1993**.

[21] D. A. Cardwell, Y.-h. Shi, N. H. Babu, S. K. Pathak, and A. R. Dennis, "Top seeded melt growth of Gd – Ba – Cu – O," **2010**. DOI: 10.1088/0953-2048/23/3/034008.

[22] S.Jin, "Melt Texture Growth: Related Process and Its Characterization," *Advances in Superconductivity II*, **1989**, pp. 257–262.

[23] Z. Lian, Z. Pingxiang, J. Ping, and W. Keguang, "The properties of YBCO superconductors prepared by a new approach: the 'powder melting process'," **1990**.

[24] S.-y. Aoki, T. Yamaguchi, Y. Ijima, A. Kagawa, O. Kohno, S. Nagayaa, and T. Inoue, "High Jc Y-Ba-Cu-O Thin Film on Metal Substrates Prepared by Chemical Vapor Deposition," vol. 547, **1992**.

[25] B Utz, R Semerad, S Rieder-Zecha, E Kobler, P Berberich, and H Kinder, "YBCO Deposition by Thermal Evaporation," *Advances in Cryogenic Engineering Materials*, U. B. Balachandran, D. G. Gubser, K. T. Hartwig, R. P. Reed, W. H. Warnes, and V. A. Bardos, Eds. Boston, MA: Springer US, **1998**, pp. 819–826.

[26] M. W. Rupich, D. T. Verebelyi, W. Zhang, and T. Kodenkandath, "M etalorganic Deposition of YBCO Films for Superconductor Wires,"

[27] B. Redwood, F. Schoffer, and B. Garret, "The 3D Printing Handbook," **2017**.

[28] K. Mikula, D. Skrzypczak, G. Izydorczyk, J. Warchoł, K. Moustakas, K. Chojnacka, and A. Witek-Krowiak, "3D printing filament as a second life of waste plastics—a review," *Environmental Science and Pollution Research*, **2020**.

[29] X. Wei, R. S. Nagarajan, E. Peng, J. Xue, J. Wang, and J. Ding, "Fabrication of YBa2Cu3O7-x (YBCO) superconductor bulk structures by extrusion freeforming," *Ceramics International*, vol. 42, no. 14, pp. 15 836–15 842, **2016**. [Online]. Available: http://dx.doi.org/10.1016/j.ceramint.2016.07.052.

[30] H. H. Xu, L. Cheng, S. B. Yan, D. J. Yu, L. S. Guo, and X. Yao, "Recycling failed bulk YBCO superconductors using the NdBCO/YBCO/MgO film-seeded top-seeded melt growth method," *Journal of Applied Physics*, vol. 111, no. 10, **2012**.

[31] K. Iida, K. Löwe, L. Kühn, K. Nenkov, G. Fuchs, G. Krabbes, G. Behr, B. Holzapfel, and L. Schultz, "Recycling process for 123-type bulk superconductors," *Physica C: Superconductivity and its Applications*, vol. 469, no. 15-20, pp. 1153–1156, **2009**. [Online]. Available: http://dx.doi.org/10.1016/j.physc.2009.05.196.

[32] N. R. Haddaway, S. J. Cooke, P. Lesser, B. Macura, A. E. Nilsson, J. J. Taylor, and K. Raito, "Evidence of the impacts of metal mining and the effectiveness of mining mitigation measures on social-ecological systems in Arctic and boreal regions: A systematic map protocol," *Environmental Evidence*, vol. 8, no. 1, pp. 1–11, **2019**.

[33] A. G. Stewart, "Mining is bad for health: a voyage of discovery," *Environmental Geochemistry and Health*, vol. 42, no. 4, pp. 1153–1165, **2020**.

[34] *Where's The Harm - From Materials Extraction?* [Online]. Available: http://www.electronicstakeback.com/toxics-in-electronics/wheres-the-harm-extraction/ (visited on 2021).

[35] M. Z. Gaffoor, A. L. Jarvis, E. A. Young, and D. Dorrell, "Comparison of the Effect of Graphene and Graphene Oxide Doping on YBCO," *Journal of Physics: Conference Series*, vol. 1559, no. 1, **2020**, ISSN: 17426596.

[36] A. Staneva, J. Mateeva, B. Martinov, B. Blagoev, and T. Nurgaliev, "EFFECT OF GRAPHENE OXIDE AND REDUSED GRAPHENE OXIDE ON ELECTRICAL PROPERTIES OF YBCO AND YBCO / Ag COMPOSITES," pp. 359–366, **2019**.

[37] S. Dadras, S. Falahati, and S. Dehghani, "Effects of graphene oxide doping on the structural and superconducting properties of YBa2Cu3O7-$\delta$," *Physica C: Superconductivity and its Applications*, vol. 548, pp. 65–67, **2018**.

[38] H. Zhang, Y. Zhao, and W. Wang, "Fe-doped epitaxial YBCO films prepared by chemical solution deposition," **2014**.

[39] S. N. Abd-Ghani, R. Abd-Shukor, and W. Kong, "Effects of Fe 3O 4 nano particles addition in high temperature superconductor YBa 2Cu 3O 7-$\delta$," *Advanced Materials Research*, vol. 501, pp. 309–313, **2012**.

[40] L Shlyk, G. Krabbes, G. Fuchs, and K. Nenkov, "Melt-processed YBCO doped with Ca and Cd : comparison of superconducting properties," vol. 383, pp. 175–182, **2002**.

[41] X Yao, D. X. Huang, K Nomura, Y Nakamura, T Izumi, and Y Shiohara, "Superconducting properties of Ca-doped YBCO thick film by liquid phase epitaxy," vol. 381, pp. 107–111, **2002**.

[42] R. Giri, H. K. Singh, O. N. Srivastava, V. P. S. Awana, A. Grupta, B. V. Kumaraswamy, and H. Kishan, "Effect of Ca doping for Y on structural / microstructural and superconducting properties of YBa 2 Cu 3 O 7-," **2005**.

[43] N. Hari Babu, M. Kambara, J. McCrone, J. R. Cooper, J. L. Talion, and D. A. Cardwell, "Fabrication of Ca-doped large grain Y-Ba-Cu-O superconductors," *IEEE Transactions on Applied Superconductivity*, vol. 11, no. 1 III, pp. 3521–3524, **2001**, ISSN: 10518223. DOI: 10.1109/77.919823.

[44] F. Licci, P. Tissot, and H. J. Scheel, "Data on the YBa2Cu3O7 - x-CuOx phase diagram," *Journal of The Less-Common Metals*, vol. 150, no. C, pp. 201–206, **1989**.

[45] B. N. Sun, P. Hartman, C. F. Woensdregt, and H. Schmid, "Structural morphology of YBa2Cu3O7-x," *Journal of Crystal Growth*, vol. 100, no. 3, pp. 605–614, **1990**, ISSN: 00220248. DOI: 10.1016/0022-0248(90)90259-N.

[46] L. Li, C. Q. Guo, J. X. Han, Y. Yan, W. T. Jin, S. J. Hao, F. Lin, K. Wei, and H. Zhang, "Role of lattice in YBCO superconductors studied by Raman spectroscopy," *International Journal of Modern Physics B*, vol. 29, no. 25-26, pp. 1–5, **2015**, ISSN: 17936578. DOI: 10.1142/S0217979215420047.

[47] C. Thomsen and G. Kaczmarczyk, "Vibrational Raman Spectroscopy of High-temperature Superconductors," *Handbook of Vibrational Spectroscopy*, **2006**. DOI: 10.1002/0470027320.s6305.

[48] R. Mohan, K. Singh, N. Kaur, S. Bhattacharya, M. Dixit, N. K. Gaur, V. Shelke, S. K. Gupta, and R. K. Singh, "Calcium and oxygen doping in YBa 2 Cu 3 O y," vol. 141, pp. 605–609, **2007**.

[49] N. M. Hidayah, W. W. Liu, C. W. Lai, N. Z. Noriman, C. S. Khe, U. Hashim, and H. C. Lee, "Comparison on graphite, graphene oxide and reduced graphene oxide: Synthesis and characterization," *AIP Conference Proceedings*, vol. 1892, **2017**, ISSN: 15517616. DOI: 10.1063/1.5005764.

[50] Horiba, *Raman Spectroscopy of Graphene*, **2013**. [Online]. Available: https://www.azom.com/article.aspx?ArticleID=10130 (visited on 2021).

Appendix A

# Appendix

## A.1 Materials

The materials used for doping can be seen in Table A.1 and the materials used for pastes in Table A.2.

Table A.1: Materials used for doping.

| Name | Brand | Purity |
|---|---|---|
| Calcium chloride dihydrate | Sigma Aldrich | ACS reagent $\geq$ 99% |
| Iron(III) oxide nanopowder | Sigma Aldrich | - |
| Graphene* | - | - |

*Graphene was produced by adding 10g of graphite and 750 ml of acetone and 250 ml of milipore in an ultrasound bath for 4 hours.

Table A.2: Materials used for the pastes.

| Name | Brand | Purity | Country |
|---|---|---|---|
| Ammonium citrate dibasic | Sigma-Aldrich | 98% | USA |
| Ammonia solution 25% | LabChem | - | Portugal |
| Calcium chloride dihydrate | Sigma-Aldrich | $\geq$ 99% | Germany |
| Dichloromethane | Honeywell | $\geq$ 99.9% | Germany |
| Dimethylacetamide | Carlo Ebra | for analysis | France |
| Dimethylformamide (DMF) | Carlo Ebra | for analysis | France |
| Ethanol | LabChem | $\geq$ 96% | Portugal |
| Ethanolamine | Sigma-Aldrich | $\geq$ 98% | Germany |
| Oleic Acid | Aldrich | technical grade, 90% | Belgium |
| Oleylamine | Aldrich | technical grade,70% | Netherlands |
| o-Xylene | Carlo Erba | For analysis | France |
| Poly(diallyldimethylammoniumchloride) solution | Aldrich | - | USA |
| Poly(ethylene glycol) | Sigma-Aldrich | - | Germany |
| Poly(methyl methacrylate) | Aldrich | - | Germany |
| Poly(vinyl alcohol) (PVA) | Aldrich | - | USA |
| Poly(vinylidene fluoride) (PFDV) | Alfa Aesar | - | Germany |
| Polysorbate 80 | Sigma-Aldrich | - | Switzerland |
| Polystyrene | Aldrich | - | USA |
| Propylene glycol | (purchase from the local pharmacy) | - | - |
| Sodium Dodecyl Sulfate (SDS) | Sigma | $\geq$ 99% | China |
| Stearic Acid | Sigma-Aldric | reagent grade, 95% | Malaysia |

## A.2 Methods

### A.2.1 Heating Treatments

The heating treatments, corresponding temperatures, oven's name and nomenclature can be seen in Table A.3.

Table A.3: Heating treatments with respective temperature and oven's name.

| Oven | Oven's Name | Heating Curve | X |
|---|---|---|---|
| FA | Termolab | 0 °C - X °C (450 °C/h)<br>X °C - X °C (14h) | 950 |
| FG | Barracha | 0 °C - X °C (450 °C/h)<br>X °C - X °C (14h) | 950 |
| NFA | Nabertherm GmbH | 0 °C - X °C (14h)<br>X °C - X °C (15h)<br>X °C - 0 °C (150 °C/h) | 900, 950, 1100 |
| NFN | Nabertherm GmbH | 0 °C - X °C (450ºC/h)<br>X °C - X °C (14h) | 900, 950 |
| NFP | Nabertherm GmbH | 0 °C - X °C (3h)<br>X °C - X °C (3h)<br>X °C - 0 °C (150 °C/h) | 950 |

### A.2.2 Spectroscopy

Equation A.1 shows the function used to normalize the reflectance results. This function relates a chosen reflectance value (RefValue) with the Reflectance minimum value (min(RefValue)) and maximum value (max(RefValue)), giving a normalized reflectance value (NormValue).

$$NormValue = \frac{RefValue - min(RefValue)}{max(RefValue) - min(RefValue)} \tag{A.1}$$

### A.2.3 Electric Measurements

The electric properties of the material were obtained by measuring Current (I) versus Voltage (V). Due to the ceramic character of the YBCO samples, the metal contacts for electrical measurements were not possible to weld and therefore, it was decided to press metal Cu wires or tape on both faces of the sample as schematized in Figure A.1 A. It was also tested the contacts directly in contact with the samples and the setup immersed in liquid nitrogen.

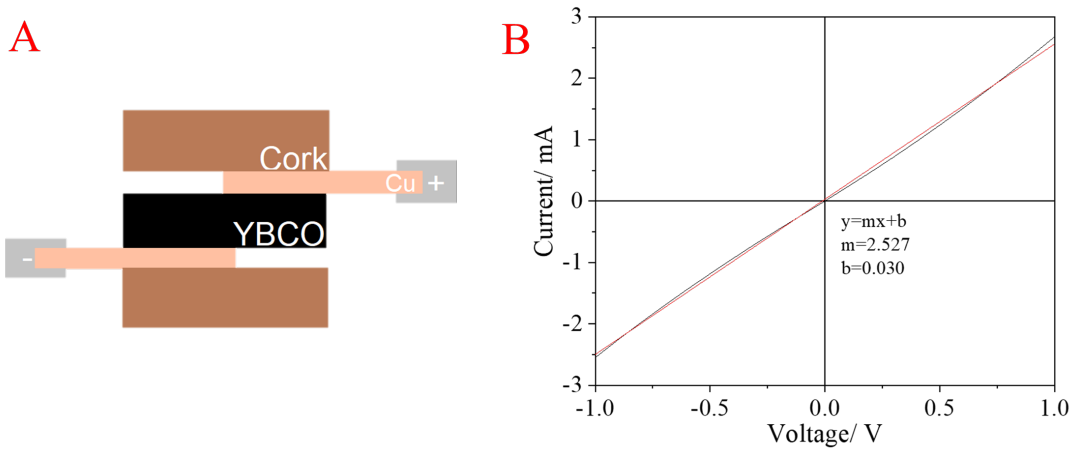


Figure A.1: A - Representation of the setup used for the electrical measurements, B - Representation of the resistivity calculation.

The material's resistance (R) was obtained from the slope of the I-V curve (Equation A.2). This can be seen in Figure A.1 B.

$$V = RI \tag{A.2}$$

The material's resistivity (ρ), is related with R, the sample's length (L) and cross-sectional area (A). The conductivity (σ) is the inverse of resistivity and both formulas can be seen in Equation A.3 and Equation A.4

$$R = \frac{L\rho}{A} \tag{A.3}$$

$$\sigma = \frac{1}{\rho} \tag{A.4}$$

### A.2.4 Magnetic Levitation

The setup of the magnetic levitation can be seen in Figure A.2.


Figure A.2: Representation of the set up used for the levitation test performance.

## A.3 Powders

The complete list of synthesized and milled powders can be seen in Table A.4 and Table A.5. In Table A.4 it is possible to see the powders mixtures, heating treatment, if they showed the presence of peak around 500 nm in the reflectance graph (characteristic of green phase), their structure (if orthorhombic or tetragonal) and their ability to levitate.

Table A.4: Description of the synthesis of the original synthesized samples as well as the presence of green phase, their structure and their ability to levitate.

| Powder | Mix | Heating Treatment | Green Phase | Structure | Levitation |
|---|---|---|---|---|---|
| O1 | A | NFA at 950 °C | - | - | - |
| O2 | A | NFA at 950 °C | - | - | - |
| O3 | A | NFA at 950 °C | - | - | - |
| O4 | A | NFA at 950 °C | - | - | - |
| O5 | B | NFA at 950 °C | - | - | - |
| O6 | A | NFA at 950 °C | - | - | - |
| O7 | B | NFA at 950 °C | - | - | N |
| O8 | A | NFA at 950 °C | - | - | Y |
| O9 | B | NFA at 950 °C | - | - | N |
| O10 | A | NFA at 950 °C | - | - | - |
| O11 | B | NFA at 950 °C | - | - | - |
| O12 | A | NFA at 900 °C | Y | O | N |
| O13 | B | NFA at 900 °C | N | O | Y |
| O14 | B | NFA at 900 °C | Y | O + T | N |
| O15 | B | NFA at 900 °C | Y | O | N |
| O16 | B | NFA at 950 °C | - | - | - |
| O17 | B | NFA at 950 °C | - | - | - |
| O18 | A | - | - | - | - |
| O19 | B | - | - | - | - |
| O20 | A | NFA at 950 °C | - | - | - |
| O21 | B | NFA at 900 °C | - | - | - |
| O22 | B | NFA at 900 °C | - | - | - |
| O23 | B | NFN at 900 °C | N | - | Y |
| O24 | A | NFA at 1100 °C | Y | - | N |
| O25 | A | FG at 950 °C and NFN at 900 °C | N | - | N |
| O26 | A | NFA at 950 °C and NFN at 900 °C | N | - | Y |
| O27 | A | FG at 950 °C | - | - | - |
| O28 | B | NFN at 900 °C | Y | - | N |
| O29 | B | NFN at 900 °C | - | - | - |
| O30 | B | NFN at 900 °C | - | - | - |
| O31 | B | NFN at 900 °C | Y | T | N |
| O32 | B | NFN at 900 °C | - | - | - |
| O33 | B | NFN at 900 °C | Y | - | N |
| O34 | B | NFN at 900 °C | Y | O + T | N |

Table A.5 shows the original powders that were milled, their milling time, the presence of the characteristic green phase peak around 500 nm, their structure (if orthorhombic or tetragonal) and their ability to levitate.

Table A.5: List of the milled powders, as well as the powders used, milling time, presence of green phase, their structure and ability to levitate.

| Powder | Original Powders | Milling Time/ min | Green Phase | Structure | Levitation |
|---|---|---|---|---|---|
| MO1 | O2, O4, O6, O8, O10 | 10 | Y | - | Y |
| MO2 | O9, O11 | 10 | Y | T | N |
| MO3 | O27 | 180 | - | - | Y |
| MO4 | O23 | 180 | - | - | Y |

## A.4 Recycled Powders

Table A.6 shows the recycled powders as well as the original powder, milling time used, if they possessed green phase (by looking at the normalized reflectance graph), their structure (if tetragonal or orthorhombic) and their ability to levitate.

Table A.6: List of the recycled milled powders, as well as the original powders, milling time, presence of green phase, structure and ability to levitate.

| Powder | Original Sample | Milling Time/ min | Green Phase | Structure | Levitation |
|---|---|---|---|---|---|
| MR1 | Mendes' samples | 10 | - | T | N |
| MR2 | Mendes' samples | 10 | N | T | N |
| MR3 | Random printed samples | 180 | - | - | - |
| MR5 | Random printed samples | 180 | N | - | N |
| MR6 | Mendes' samples | 180 | - | - | N |
| MR7 | Mendes' samples | 180 | N | - | Y |

## A.5 Doped Powders

This section shows the tables for the doped powders. Table A.7 to Table A.9 show the original mixture, doping agent and content.

Table A.7: List of the Ca(II) doped samples with doping agent and content.

| Powder | Original Mixture | Doping agent | Doping quantity/wt% |
|---|---|---|---|
| CaO21 | B | $CaCl_2$ | 0.05 |
| CaO22 | B | $CaCl_2$ | 0.10 |
| CaO23 | B | $CaCl_2$ | 0.15 |
| CaO24 | B | $CaCl_2$ | 0.20 |
| CaO25 | B | $CaCl_2$ | 0.30 |

Table A.8: List of Fe(III) doped samples with doping agent and content.

| Powder | Original Powder | Doping agent | Doping quantity/wt% |
|---|---|---|---|
| FO21 | B | $Fe_2O_3$ | 0.01 |
| FO22 | B | $Fe_2O_3$ | 0.02 |
| FO23 | B | $Fe_2O_3$ | 0.03 |
| FO24 | B | $Fe_2O_3$ | 0.04 |
| FO25 | B | $Fe_2O_3$ | 0.05 |

Table A.9: List of rGO doped samples with doping agent and content.

| Powder | Original Powder | Doping agent | Doping quantity/wt% |
|---|---|---|---|
| GO21 | B | rGO | 0.1 |
| GO22 | B | rGO | 0.3 |
| GO23 | B | rGO | 0.7 |
| GO24 | B | rGO | 1.0 |

## A.6 Material Synthesis

Different surfaces and different surface placement were tested in order to see if its placement or the material of the surface influenced the final product. It was seen that the placement of the surface did influence the heating of the sample inside the oven, probably due to convection currents. The best position is the one represented in Figure A.3.

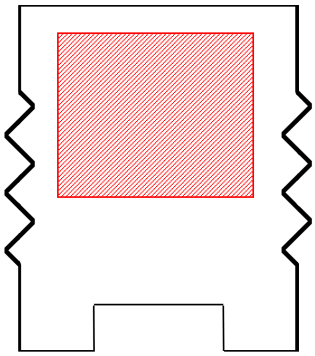

Figure A.3: Representation of the oven's interior.

For the material used, neither alumina or stoneware seemed to have a big influence on the final product but it would be best to use alumina surfaces to prevent possible contaminations.

## A.7 Electrical Measurements

Table A.10 shows the comparison between samples and their electric measurements. It also shows if they were recycled and their original powder, if they were doped and if so, their doping agent and content, the temperature and heating treatment, the mixture used, what contacts were used and the conductivity measured.

Table A.10: Electric measurements comparison.

| Sample | Recycled | Original Powder | Doping Agent and Content | Temperature and Treatment | Mixture | Contacts | Conductivity (S/m) |
|---|---|---|---|---|---|---|---|
| MR7 | Y | Mendes' | - | - | - | tape | $1.26x10^{1}$ |
| O33 | N | - | - | 900 °C NFA | B | tape | $3.09x10^{0}$ |
| GO23 | N | - | rGO 0.7 | 900 °C NFN | B | tape | $2.40x10^{0}$ |
| FeO24 | N | - | Fe 0.04 | 900 °C NFN | B | tape | $1.84x10^{0}$ |
| O34 | N | - | - | 900 °C NFA | B | tape | $1.69x10^{0}$ |
| O31 | N | - | - | 900 °C NFN | B | tape | $1.38x10^{0}$ |
| GO24 | N | - | rGO 1.0 | 900 °C NFN | B | tape | $1.17x10^{0}$ |
| CaO22 | N | - | Ca 0.1 | 900 °C NFN | B | tape | $1.11x10^{0}$ |
| GO21 | N | - | rGO 0.05 | 900 °C NFN | B | tape | $1.09x10^{0}$ |
| CaO24 | N | - | Ca 0.2 | 900 °C NFN | B | tape | $1.05x10^{0}$ |
| FeO21 | N | - | Fe 0.01 | 900 °C NFN | B | tape | $9.99x10^{-1}$ |
| O28 2 | Y | O28 1 | - | - | - | tape | $9.30x10^{-1}$ |
| FeO22 | N | - | Fe 0.02 | 900 °C NFN | B | tape | $8.38x10^{-1}$ |
| O28 1 | N | - | - | 900 °C NFN | B | tape | $7.83x10^{-1}$ |
| FeO25 | N | - | Fe 0.05 | 900 °C | B | tape | $6.95x10^{-1}$ |
| MR2 | Y | Mendes' | - | - | - | tape | $4.31x10^{-1}$ |
| CaO25 | N | - | Ca 0.3 | 900 °C NFN | B | tape | $3.56x10^{-1}$ |
| O131 | N | - | - | 900 °C NFA | B | tape | $2.81x10^{-1}$ |
| O151 | N | - | - | 900 °C NFA | B | wire | $2.15x10^{-1}$ |
| CaO23 | N | - | Ca 0.15 | 900 °C NFN | B | tape | $1.65x10^{-1}$ |
| O121 | N | - | - | 900 °C NFA | A | wire | $1.21x10^{-1}$ |
| O141 | N | - | - | 900 °C NFA | B | wire | $8.06x10^{-2}$ |
| MO1 | N | - | - | - | A | wire | $4.42x10^{-2}$ |
| FeO23 | N | - | Fe 0.03 | 900 °C NFN | B | tape | $9.13x10^{-3}$ |
| MO2 | N | - | - | - | B | tape | $1.76x10^{-3}$ |
| MR6 | Y | Mendes' | - | - | - | tape | $1.97x10^{-4}$ |

## A.8 Bean Critical State Model Values

The values used for the calculation of $J_C$ using the Bean critical state model can be seen in Table A.11.

Table A.11: Values used for the Bean critical state model.

| | O121 | | | O131 | | | MR7 | | |
|---|---|---|---|---|---|---|---|---|---|
| T | ΔM | a | b | ΔM | a | b | ΔM | a | b |
| 77 | 0.650 | 5 | 5 | 1.152 | 5 | 5 | 2.0 | 3 | 4 |
| 50 | 1.124 | | | 3.347 | | | 5.2 | | |
| 10 | 5.776 | | | 10.778 | | | 17.4 | | |
| 4 | 8.799 | | | 14.606 | | | 24.4 | | |

## A.9 Levitation Performance

Table A.12 shows the levitation performance of synthesized samples, as well as the original powder used, mixture, heat treatment and respective temperature and the presence of green phase and structure (if orthorhombic or tetragonal).

Table A.12: Levitation table - synthesized samples.

| Sample | Levitate | Original Powder | Mix | Heat Treatment | Green Phase | Structure |
|---|---|---|---|---|---|---|
| O7 | N | - | B | 950 °C NFA | - | - |
| O8 | Y | - | A | 950 °CNFA | - | - |
| O9 | N | - | B | 950 °C NFA | - | - |
| O12 | N | - | A | 900 °C NFA | Y | O |
| O13 | Y | - | B | 900 °C NFA | N | O |
| O14 | N | - | B | 900 °C NFA | Y | O + T |
| O15 | N | - | B | 900 °C NFA | Y | O |
| O23 | N | - | B | 900 °C NFA | N | - |
| O24 | N | - | B | 1100 °C NFA | Y | - |
| O25 | N | - | A | 950 °C FG | N | - |
| O26 | Y | - | A | 950 °C FA + 900 °C NFN | N | - |
| O28 1 | N | - | B | 900 °C NFN | Y | ? |
| O31 | N | - | B | 900 °C NFN | N | T |
| O33 | N | - | B | 900 °C NFN | Y | ? |
| O34 | N | - | B | 900 °C NFN | Y | O + T |
| MO1 | Y | O10, O8, O6, O4, O2 | - | 950 °C NFA | Y | - |
| MO2 | N | O11, O9 | - | 900 °C NFA | Y | T |
| MO3 | Y | O27 | - | 950 °C FG | - | - |
| MO4 | Y | O23 | - | 900 °C FG | - | - |

Table A.13 show the levitation performance table for the recycled samples, as well as the original powder used, heat treatment and respective temperature, the presence of green phase, and structure (if tetragonal or orthorhombic).

Table A.13: Levitation table - recycled samples.

| Sample | Levitate | Original Powder | Heat Treatment | Green Phase | Structure |
|---|---|---|---|---|---|
| MR1 | Y | Mendes' pieces | NFA at 950 °C | - | T |
| MR2 | N | Mendes' pieces | NFA at 950 °C | N | T |
| MR5 | N | Random printed samples | - | N | - |
| MR6 | - | Mendes' pieces | NFN at 900 °C | - | ? |
| MR7 | Y | Mendes' pieces | NFN at 900 °C | N | ? |

Table A.14 to Table A.16 show the levitation performance table for the doped samples. In them it is also possible to see the mixture used, the heat treatment and temperature, the presence of green phase and the present structure (orthorhombic and tetragonal).

Table A.14: Levitation table - calcium(II) doped samples.

| Sample | Levitate | Mix | Heat Treatment | Green Phase | Structure |
|---|---|---|---|---|---|
| CaO21 | N | B | NFN at 900 °C | - | O + T |
| CaO25 | N | B | NFN at 900 °C | Y | T |

Table A.15: Levitation table - iron(III) doped.

| Sample | Levitate | Mix | Heat Treatment | Green Phase | Structure |
|---|---|---|---|---|---|
| FeO21 | N | B | NFN at 900 °C | Y | ? |
| FeO25 | N | B | NFN at 900 °C | Y | ? |

Table A.16: Levitation table - graphene doped samples.

| Sample | Levitate | Mix | Heat Treatment | Green Phase | Structure |
|---|---|---|---|---|---|
| GO21 | N | B | NFN at 900 °C | Y | T |
| GO24 | N | B | NFN at 900 °C | Y | O + T |

## A.10 3D Printing

Table A.17 and Table A.18 show the list of pastes that failed the extrusion and printing tests. It also shows the powders used, what test was failed and the issue behind it.

Table A.17: List of Pastes that failed the extrusion and printing tests with the powder used and its issues.

| Paste | Powder | Extrudable | Printable | Issue |
|---|---|---|---|---|
| xylene, PS, oleylamine, oleic acid | MO1 | Y | N | uses too much material and solidifies quickly |
| ethanolamine | O25, MR3 | Y | N | ethanolamine reacts with YBCO |
| ammonium citrate dibasic, milipore | O25, MO4, O28 1 | N | N | creates clusters and promote phase separation |
| DMF, PVDF, polysorbate 80 | O28 1, MR5 | N | - | can not be extruded |
| cyclohexane, PS | MO4, O28 1 | Y | N | solidifies too quickly |
| PVDF, DMF | O25 | Y | N | too liquid but should be investigated with higher concentrations |
| DMF, PS | O28 1, MO4 | N | - | solidifies too quickly |
| oleylamine, acid oleic | MO1, MR1 | Y | N | lost its structure after the thermal treatment |
| oleic acid, oleylamine, ethanol, PEG | MO2, MR1 | Y | N | reacts with YBCO |
| dodecanol, stearic acid, dichloromethane | - | Y | Y | should be investigated for YBCO instead of precursors |
| poly(diallydimethylammoniumchlride) solution | Precursors MR3 | Y | N | did not levitate with the precursors nor MR3 so it must have reacted with them |
| ammonium citrate dibasic, milipore, ethanolamine | O25 | N | - | solidifies too quickly |
| PVA, milipore | MO4 | N | - | tendency to form clusters |
| milipore | MO4 | - | - | reacted harshly with water |
| oleic acid, amoniac, milipore, SDS | MR1 | Y | Y | lost its structure after the thermal treatment |

Table A.18: Pastes failed - continuation.

| Paste | Powder | Extrudable | Printable | Issue |
|---|---|---|---|---|
| PE, ethanol, oleic acid | MR1 | Y | N | solidifies too quickly |
| oleic acid, oleic acid and ammonia mix, amoniac | MR1 | N | N | too liquid but should be investigated with higher concentrations |
| oleic acid, ethylene glycol | MR1 | N | N | too solid to print or extrude |
| oleic acid, oleylamine, amoniac, milipore, SDS | MR1 | Y | Y | lost its structure after the thermal treatment |
| DMAC, PS | MR1 | N | N | too solid to print or extrude |
| PMMA, DMAC, acetone | MR2 | N | N | too liquid but should be investigated with higher concentrations |

## A.11 Raman Photos

In Figure A.4 to Figure A.6 it is possible to see the photos taken of the samples and the regions that were chosen for the Raman spectroscopy.

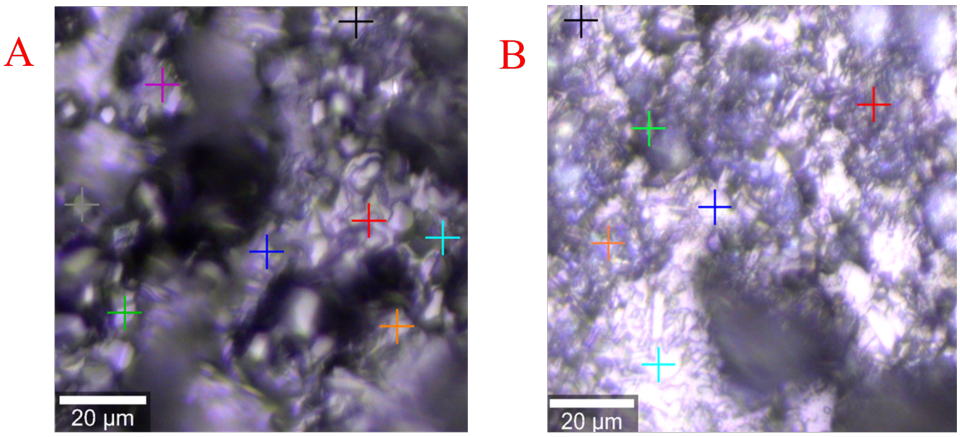


Figure A.4: Raman photos of Ca(II) doped YBCO samples with A - 0.1wt% and B - 0.3wt%.

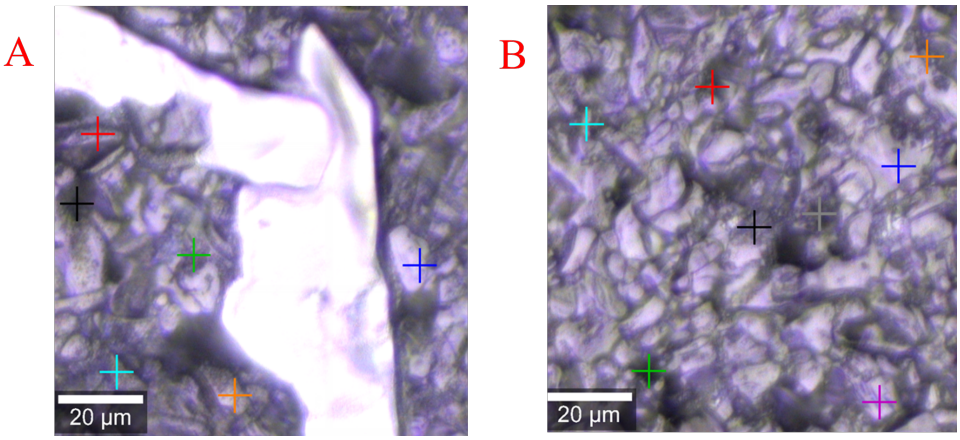


Figure A.5: Raman photos of graphene doped YBCO samples with A - 0.1wt% and B - 1.0wt%.

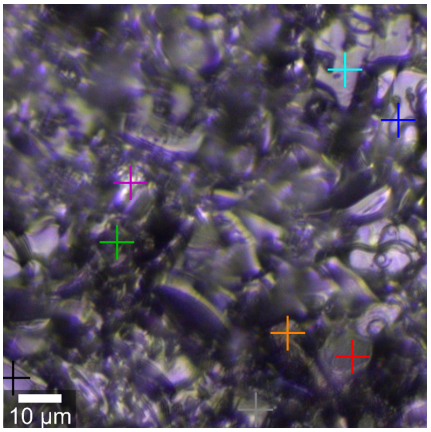


Figure A.6: Raman photos of Fe(III) doped YBCO samples with 0.05wt%.

## A.12 Spectroscopy

Figure A.7 to Figure A.9 show the Normalized Reflectance spectra of several samples in order to see if they had the presence of the peak at 500 nm (characteristic of the green phase) and if they levitated.

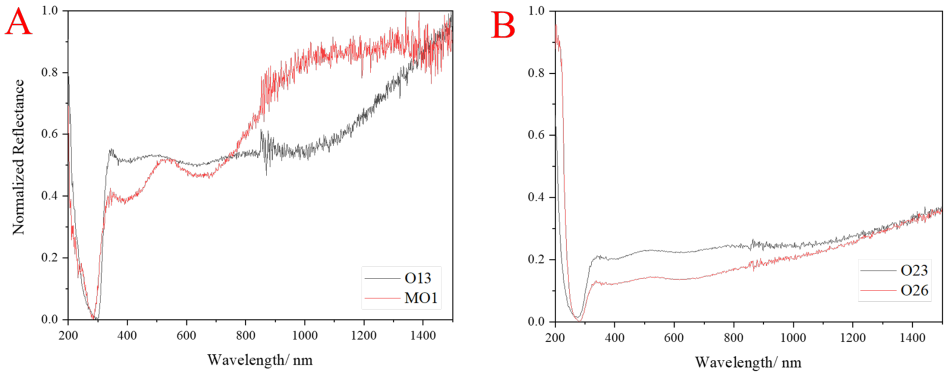


Figure A.7: Normalized reflectance spectra of samples A - O13, MO1 and B - O23, O26 that had the ability to levitate.

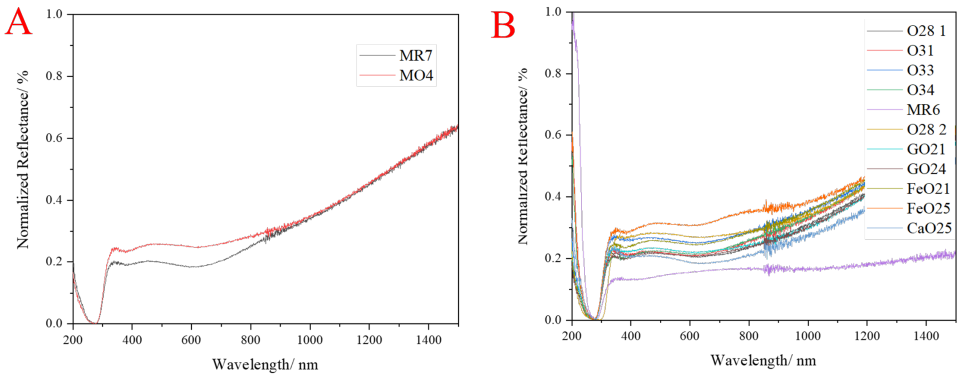


Figure A.8: Normalized reflectance spectra of samples A- MR7, MO4 that had ability to levitate and B - O28 1, O31, O33, O34, MR6, O28 2, GO21, GO24, FeO21, FeO25, CaO25 that did not have the ability to levitate.

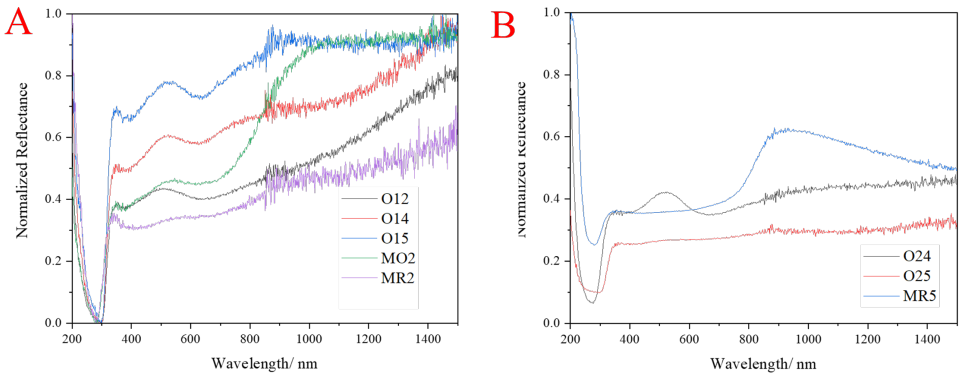


Figure A.9: Normalized reflectance spectra of samples A- O12, O14, O15, MO2, MR2, B - O24, O25, MR5 that did not have the ability to levitate.

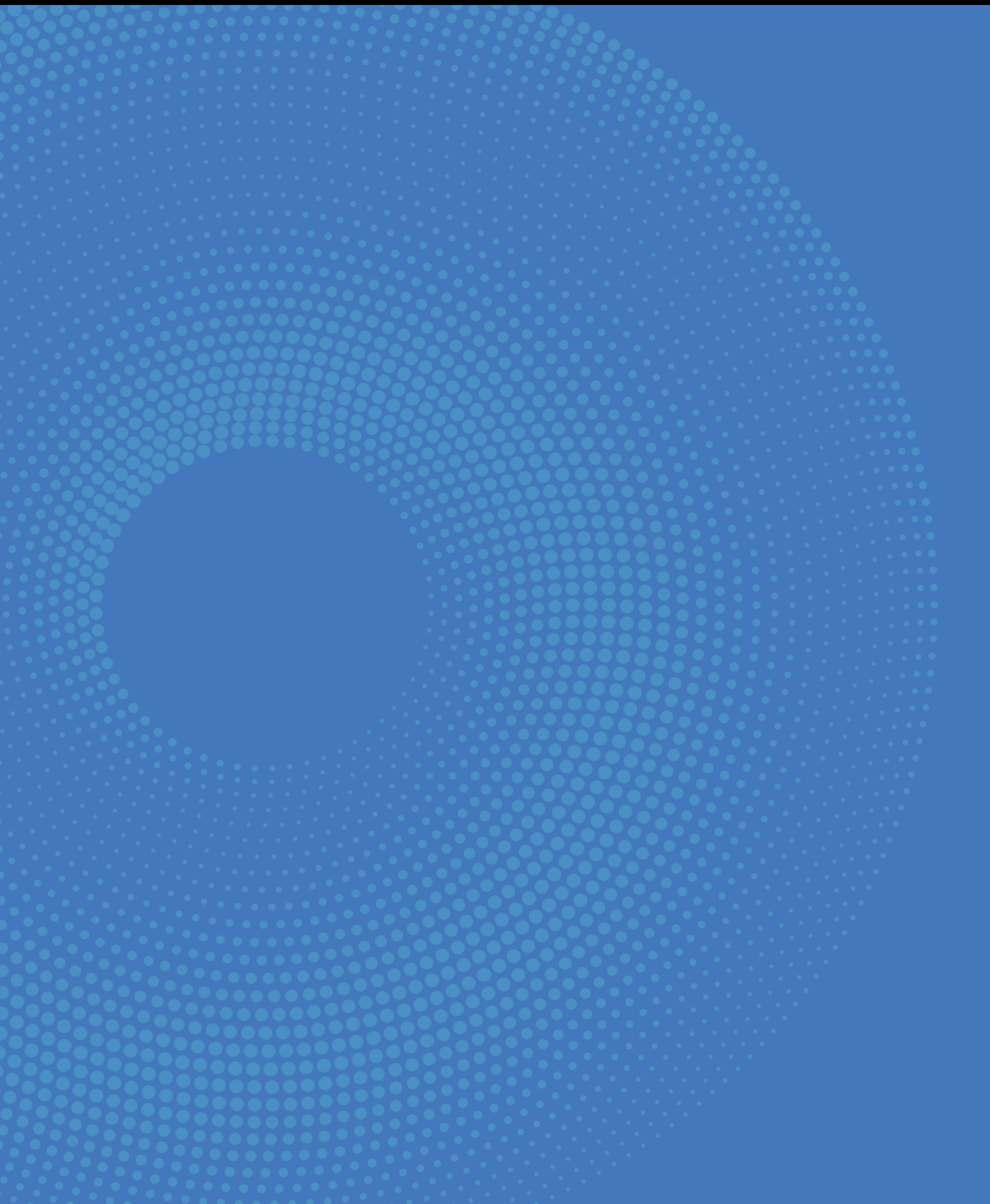

2021

MARIA TERESA OLIVEIRA PULQUÉRIO
DE SILVEIRA

# 3D PRINTING OF YBCO-BASED SUPERCONDUCTORS

NOVA SCHOOL OF
SCIENCE & TECHNOLOGY